Alexandria Engineering Journal (2023) 74, 241–268

HOSTED BY

Alexandria University

Alexandria Engineering Journal

www.elsevier.com/locate/aej
www.sciencedirect.com

ORIGINAL ARTICLE

Validation hybrid filter detection for Multi-User multiple input multiple output F-OFDM by Universal software radio Peripheral

Waleed Algriree [a,*], H. alsheakh [b], Nasri Sulaiman [c,*], Maryam Isa [c], Ratna K. Z. Sahbudin [a], Siti L. M. Hassan [d], Emad Hmood Salman [e]

[a] *Department of Computer and Communication Systems Engineering, Faculty of Engineering, Universiti Putra Malaysia, Serdang 43400, Selangor, Malaysia*
[b] *Clinical laboratory sciences, college of Pharmacy, University of mustansiriyah, Qadisiya HW, Baghdad, Iraq*
[c] *Department of Electrical and Electronic Engineering, Faculty of Engineering, Universiti Putra Malaysia, Serdang 43400, Selangor, Malaysia*
[d] *Faculty of Electrical Engineering, Universiti Teknologi MARA, Selangor, Malaysia*
[e] *Department of Communications Engineering, College of Engineering, University of Diyala, Baquba 32001, Diyala, Iraq*

Received 26 January 2023; revised 3 April 2023; accepted 16 April 2023

KEYWORDS

5G Environment;
Hybrid filter detection;
MIMO-F-OFDM;
Cognitive radio;
Spectrum sensing;
USRP B210;
GNU Radio;
Monte-Carlo;
QAM

Abstract The present communication system is not enough efficient for the data rate requirement for the real-time applications like video conferencing and file sharing. To meet the requirement of the data rate, the concept of F-OFDM (Filter- Orthogonal Frequency Division Multiplexing) has been proposed. To further improve the efficiency of the system, Cognitive Radio is used. Cognitive Radio is capable of recognizing the spectrum utilization of the licensed users and accordingly switches the frequency bands. The aim of the paper is to detect the primary users in an efficient and novel way. Therefore, a hybrid filter detection technique is proposed for the Multi-User Multiple Input Multiple Output (MU-MIMO) F-OFDM system where multiple users are served with the same time and frequency resource and improve signal strength. The proposed technique uses the combination of cosine filtering, Bartlett segmenting, and Hamming windowing. The cosine filtering differentiated between the 5G traffic and the noise. Then, the filtered signals are segmented with the help of the Bartlett Segmenting for decreasing the noise variance then every segment is windowed using the Hamming windowing for maintaining the signal resolution. This paper proposes a Validation Hybrid Filter Detection for Multi-User Multiple Input Multiple Output (MIMO) Frequency-Division Multiplexing Orthogonal Frequency Division Multiplexing (F-OFDM) by Universal Software Radio Peripheral (USRP) based on Cognitive Radio (CR). Detection performance dropped to its least value for M−ary = 256 and 10 user SUs. Further, false alarm proba-

* Corresponding authors.
E-mail addresses: wkh_portsmouth@yahoo.com (W. Algriree), Hussein.alsheakh@uomustansiriyah.edu.iq (H. alsheakh), nasri_sulaiman@upm.edu.my (N. Sulaiman), maryam@upm.edu.my (M. Isa), ratna@upm.edu.my (R. K. Z. Sahbudin), sitilailatul.mohdhassan@yahoo.com (S. L. M. Hassan), emad_salman_eng@uodiyala.edu.iq (E.H. Salman).

Peer review under responsibility of Faculty of Engineering, Alexandria University.

https://doi.org/10.1016/j.aej.2023.04.033

bility at −24 dB SNR was less than 0.01, which is excellent considering system characteristics of less than 0 dB SNR, 0.092% and > 98% global system error and detection likelihoods, respectively. The study also evaluated spectral efficiency to offer optimum detection at acceptable complexity levels for low SNR signals. The performance of the proposed technique is compared with the existing techniques and it is found that the proposed technique better and can effectively improve the detection accuracy of the signal with low SNR.

1. Introduction

Recent times have witnessed rapid increases in data and throughput demand. 5G and future wireless networks must enable several services like the internet of things, dynamic spectrum utilization and machine interaction at scale to satisfy these demands [1]. To meet these demands, 5G and future networks must support several new technologies such as cognitive radio, dynamic spectrum utilization, massive MIMO, beamforming, and mmWave communication. Dynamic spectrum utilization allows for efficient reuse of spectrum resources, allowing for increased capacity and efficiency. Massive MIMO enables spatial multiplexing, allowing for transmission of multiple data streams over the same frequency. Beamforming allows for energy to be focused in the direction of the receiver, resulting in increased signal reception. Lastly, the use of mmWave frequencies enables higher data rates than are possible with traditional sub-6 GHz frequencies [2 3 4 5]. All of these technologies must be implemented together in order to enable 5G and future networks to meet the high throughput and data demands of today. The combination of these technologies will enable higher data rates, increased capacity, improved power efficiency, and better coverage [6]. 5G offers better data rates at lesser latencies, better power efficiency than older networks, better network capacity, and an increased number of connections. Mobile networks are advancing rapidly; hence, the finite radio spectrum is becoming costly and scarce [7]. 5G is designed to address this issue by using a new technology called MIMO (Multiple Input Multiple Output) [8]. This technology helps to increase the capacity and speed of the network by using multiple antennas at the transmitter and the receiver. 5G also allows for higher frequency bands to be used, which allows for more data to be transmitted in shorter timeframes. Furthermore, 5G technology offers improved network reliability, lower latency, improved spectrum efficiency, and more cost-effective services [9]. Hence, Dynamic spectrum access (DSA) is an approach to wireless communication in which users access the spectrum opportunistically, taking advantage of unused parts of the spectrum. In contrast to more traditional approaches, such as frequency assignment and exclusive-use licensing, DSA does not require users to be allocated a specific frequency or band. Instead, users can exploit any available frequency or bandwidth as long as they do not cause interference to existing users. This allows for more efficient use of the spectrum, since unused channels can be utilized, while also providing more flexibility in communication networks. DSA has been applied in various types of wireless networks, including cognitive radio networks, wireless mesh networks, and mobile ad-hoc networks [10]. 5G networks are designed to leverage spectrum sensing to improve efficiency and optimize radio spectrum utilization. Spectrum sensing is a process that enables a radio receiver to measure the power of a signal in a certain frequency range and then determine whether there is an active signal in that range. It is used to detect and identify the presence of any wireless signal in the radio spectrum. Spectrum sensing can be used to identify the spectrum occupancy in a given frequency range and can be used in dynamic spectrum allocation, where communication networks can be dynamically reconfigured to use the available spectrum [11]. It is also used in spectrum sharing, where two or more wireless networks can share the same spectrum, exploiting the fact that only one network is transmitting at any given time. Spectrum sensing detection in 5G networks with low SNR (Signal-to-Noise Ratio) is a challenging task due to the high noise levels inherent in 5G networks [12]. To improve the accuracy of spectrum sensing detection with low SNR, one approach is to employ Cognitive Radio (CR) technique (spectrum sensing). The main goal is to enable SUs to use the spectrum efficiently and effectively. To achieve this, SUs must be able to sense the environment, detect available channels, and access them opportunistically. This is done by SUs detecting the presence of PUs and vacating the spectrum when a PU appears. Cognitive radio can also be used to improve spectral efficiency by allowing SUs to dynamically adjust their transmission parameters to best suit the current environment. For example, the CR system can exploit signal-to-noise ratio (SNR) measurements to determine whether or not a signal is present in a specific frequency band. If a signal is present, it can then be identified or detect it by using hybrid filter detection technique have been proposed. Furthermore, cooperative sensing between users can also be employed to further improve the accuracy of spectrum sensing.

Filtered Orthogonal Frequency Division Multiplexing (F-OFDM) has distinctive characteristics that separate it from the traditional Orthogonal Frequency Division Multiplexing (OFDM). The main advantage of F-OFDM is its improved spectral efficiency, and a better system performance. F-OFDM also has a lower computational complexity and is more resilient to frequency-selective fading. F-OFDM offers a better frequency-domain equalization and eliminates the need for a cyclic prefix. This reduces the overhead, improves the data rate, and increases spectral efficiency [13]. Lastly, F-OFDM can reduce the effect of inter-symbol interference, leading to a better signal-to-noise ratio. MIMO (Multiple Input Multiple Output) technology is a key component of 5G technology. It enables 5G networks to transmit large amounts of data at high speeds over wide areas [14]. The main advantage of MIMO is that it helps to improve the coverage, capacity, and performance of wireless networks. It also reduces interference, which helps to improve the quality of connec-

tions. Additionally, MIMO technology allows for more efficient use of spectrum and increases the capacity of a wireless network [15]. F-OFDM is the top choice for building new-generation networks' physical layer because it provides superior performance, lesser complexity, smoothness, and cost-effectiveness, as the existing spectrum cannot fulfil the 5G requirements, also to detect 5G waveform with low SNR signals using more complexity levels have been a research priority in this paper. To address this issue using hybrid filter detection (HFD) technique that is proposed to sense MIMO F-OFDM waveform based on cognitive radio network (CRN). The proposed SS technique (HFD) was dependent on the bases of cosine filters that blindly tested the white bands and differentiated between the noise and traffic signal. Additionally, the target signal was segmented after filtering using the Bartlett segmentation, and windowed using the Hamming window for maintaining the signal resolution and establish segment-specific PSD. Lastly, we compared the pre-specified limit and the PSD average (test statistic) to determine the presence of a signal. Detection happened fast, and the issue of low SNR was addressed in the context of differentiating noise and variance. Also Monte Carlo (MC) simulation was employed to verify mathematically outcomes. which alone do not suffice to prove the validity pertaining to the algorithms, and thus a case involving practical implementation is needed by employing USRP B210. Analysis of the performance of the system is done by implementing practically as it provides a realistic picture of the effectiveness pertaining to the spectrum sensing algorithm (HFD). The suggested approach was verified using National Instruments (USRP B210) system. This experiment assessed USRP flexibility, necessitating the exploration of a practical testbed comprising real-world spectrum sensing approach. The major points which must be comprehended include the SNR wall, detection probability rate, system-error probability rate, false-alarm probability rate, the PSD of Received MIMO F-OFDM for Various SNR Values, AWGN and Rayleigh channel, and computational complexity. The spectrum detection outcomes helped establish the degree of correlation between the Practical implementation and simulation. In this paper has been organized in the following manner: the introduction is presented in this section, while Section two describes main contributions, section three is presented the literature review, section four is presented the proposed CSS based 5G environment model, section five is presented impact of SNR on Received Signals, section six is presented the implementation Platform, section seven describes all the graphical and numerical results instead of analysing or discussing the results. Lastly, Section eight presents the conclusions and future works.

2. Main Contributions:

- The HFD-based spectrum detection for the National Instrument (NI) USRP, software-defined radio (SDR) system that evaluates a 600 MHz to 4.2 GHz carrier frequency range. USRP offers in-built software and hardware approaches for quick prototyping of high-performance wireless networks based on the LabVIEW interface solution.
- Moreover, a plot of the performance indicator is created with detection probability Pd and Pfa. It was noted that the ED approach performance suffers at low SNR magnitudes.
- Furthermore, we suggest using the SS approach for precise 5G signal detection to address the energy detection limitations. The recommended technique uses three processes in sequence: cosine filters (to differentiate 5G traffic from noise), Bartlett-based segmentation (i.e., segmenting the target waveform after Bartlett filtering); Bartlett segmentation lowers residual noise variance. The last process comprises the Hamming window to retain the signal resolution and establish segment-specific PSD. Lastly, we compared the prespecified limit and the PSD average (test statistic) to determine the presence of a signal. Detection happened fast, and the issue of low SNR was addressed in the context of differentiating noise and variance. The approach offers excellent performance and is blind in the true sense, i.e., it does not need prior information.
- In contrast, the sensing approach is based on MIMO cooperative spectrum for identifying F-OFDM signals comprising high throughput and appreciable performance (to enhance throughput and spectrum efficiency).
- Offer a feasible spectrum detection approach, and build hybrid filter detection for identifying 2x2 MIMO F-OFDM waveforms based on simulations and mathematics. Simulations are performed using MATLAB. The characteristics are concerning a practical 2x2 MIMO F-OFDM waveform-specific spectrum detection modules in GNU Radio Companion, deployed using the National Instruments (NI) testbed. This testbed offers ubiquitous software radio peripherals with modifiable input/out (USRP B210) base using GNU radio companion.
- Hybrid filter was used to address the noise issue. Filter length is reduced by eliminating null coefficients related to R[k] to decrease the sensing period by optimising computational requirements.
- Evaluate how M−ary rates affect signal sensing for F-OFDM MIMO systems
- Evaluate the impact error in the context of the proposed 5G waveform approach (MIMO F-OFDM)
- Evaluate the effect of overall error likelihood concerning the F-OFDM 5G signal
- Evaluate the effect of MIMO F-OFDM (ED and HFD) approaches on Rayleigh and AWGN channels concerning M−QAM
- A brief about the detailed literature review concerning detection probability (Pd) approaches based on low SNR and false alarm likelihood (Pf).

3. The literature review

The literature indicates several approaches based on the cooperative spectrum sensing technique. Performance assessment outcomes were evaluated on detection likelihood of detection miss and false alarms. In July 2018, Keesara Upender Reddy devised a detector that used autocorrelation [16] This system offers appreciable detection characteristics for low SNR regimes (-10 dB); nevertheless, it was unsuitable for lower SNR values, also increased complexity. In 2019, Kumar A. and Saha S. [17] worked on a CSS approach and assessed the likelihood ratio-specific energy evaluation model. All SUs are equipped with several sensing (2–10), including two transmission antennas. FC comprises several receiving antennas (2–

10). The evaluated technique was employed for the MIMO channel to optimize computational requirements. Sadly, it has inadequate false alarm likelihood and a high SNR wall, also it increased complexity due to the need of MIMO processing. That very year, Lee W. and Cho D. [18] devised a deep CSS technique based on convolutional neural systems. This technique effectively determines vacant frequencies on a 5G system. It was used to find an optimal K value, offering the best K-out-of-N system. A system with 32 SUs has appreciable performance; however, it drops with SNR. Finally, deep cooperative sensing is not always suitable for real-time applications, since the training process can take a long time. In 2020, Yu S. et al. [19] a CSS-based adaptive double threshold technique for the ED mechanism. The ceiling and floor levels can be regulated using the devised algorithm using weighting thresholds concerning every SU. An SNR band on −20 dB to 10 dB requires the use of the AWGN channel. Low SNRs correspond to significant performance levels (high detection likelihood). Nevertheless, performance suffers when 25 SUs operate below −15 dB SNR, also complexity system and requires more resources such as communication and computation. Additionally, the algorithm is sensitive to channel noise and requires a more accurate channel estimation in order to be effective. Finally, the algorithm may not be able to detect very small signal levels due to the double-threshold approach. In 2020, Balachander T., and Krishnan M. [20] assessed the 5G-NOMA-based CRN technique. The SS approach used CSS using a MIMO network based on AWGN and Rayleigh fading channels. Detection characteristics are appreciable for 10 SUs for high SNR; nevertheless, the system under delivers when SNR falls, also is more complex. In 2020, Giri M.K. and Majumder S. [21] devised a CSS approach using the Kernel fuzzy c-means clustering technique. This framework was contrasted using the eigenvalues concerning the signal covariance matrix-based spectrum detection. This system offered precise identification only for 12 SUs. Moreover, it fails when SNR drops below −10 dB; further, it is computationally complex. M.S. Miah [22] devised the weighted-eigenvalue detection (WEVD) approach comprising a cognitive radio sensing mechanism based on a multi-user multiple-input and multiple-output (MU-MIMO). This approach was meant for cognitive radio Internet of Things (CR-IoT) having weighted-eigenvalue detection (WEVD) to assess system data rate, detection evaluation, predicted lifetime, energy efficiency, identification fain, and enhanced system data rate; however, it was inadequate below 0 dB SNR.. In 2020, several techniques were proposed: Time-Reversal Maximal Ratio Combining (TR-MRC), Time-Reversal Widely Linear (TR-WL), and modified TR-MRC (TR-mMRC) guidelines for DF. Dey, Ciuonzo, P. Salvo Rossi devised the DF Center (DFC) approach [23] Performance enhancement is projected for TR-specific fusion guidelines than traditional rules. Nevertheless, the system failed to handle low SNR values. In 2020, T. Balachander & M.B. Mukesh Krishnan suggested using Sparse code Multiple Access (SCMA) [24] The proposal was to optimise detection characteristics and spectrum sensing for 0 to 20 dB SNR values; however, performance suffers when SNR falls. In 2021, T. Balachander & M. B. Mukesh Krishnan devised the MINO NOMA methodology [25] The proposal considers enhancing the ergodic capacity of CRN concerning Rayleigh Fading and AWGN channels. The approach is employed to enhance SU spectrum utilisation; performance is inadequate at lower SNR values. Transitioning a theoretical F-OFDM proof-of-concept to a real-world implementation is critical. Sowmiya and Sangeetha [26] assessed a CR method that used ED modulation based on USRP NI 2920 instruments. The test comprised receiving a signal modulated using the quadrature phase-shift keying (QPSK) approach. Energy assessments were used for PU identification; however, the test system failed at low SNR values. Amor Nafkha, Malek Naoues, Krzysztof Cichon and Adrian Kliks [27] proposed using cyclostationary features and sequential energy for creating detectors. The cyclostationary feature identifier is based on the GNU radio-based Universal Software Radio Peripheral platform; it offers better performance compared to the sequential energy detector. Nevertheless, the latter may be employed to sense faster when signals are strong. Detection performance is appreciable at (-5, −10, −15) dB; however, the system suffered below these SNR levels. In [28], Ching-Lun Tai, Borching Su, and Cai Jia used depth-first sphere decoding (DFSD) to build a MIMO-GFDM identification approach concerning MIMO-GFDM spatial multiplexing (SM) by employing frequency-domain (FD) decoupling. The system provided a considerable computational complexity reduction; however, it failed to detect F-OFDM signals having very low SNR. Post reviewing all of the above-mentioned techniques, the authors reached a conclusion that the SS issues cannot be addressed effectively with the help of these techniques. The key points that need to be realised are the computational complexity, detection probability rate, SNR wall, false-alarm probability rate and system-error probability rate. Thus, they put forward the SS technique called (HFD) that relied majorly on the bases of cosine filters that blindly evaluated the white bands as well as provided a differentiation between the signal and the noise. Moreover, the Bartlett segmentation was employed to divide the target signal post filtration, and windowed based on the Hamming window to maintain the signal resolution. As shown earlier, a new CSS method was developed based on the Cosine-Welch-Hamming cascaded hybrid filter. This filter has been designed to identify waveform F-OFDM, which are typically employed in 5G environment. Compressing of the active coefficients of addressed signal has been done by maintaining the signal resolution as well as decreasing the difference in noise. These paper's key contributions can be laid out as follows. First, the put forward CSS technique has been largely derived and then integrated with 5G technology-based CRNs to detect the candidate pertaining to 5G waveform F-OFDM. Second, the put forward CSS technique could sense quickly as the sensed signal was compressed, wherein the resolution pertaining to the sensed signal was preserved and the noise difference was decreased. Third, this technique was also seen to subdue the high SNR wall, i.e., it can identify changing signals for SNR = -24 dB. Furthermore, it provides higher sensing accuracy, higher sensing performance and decreased sensing error versus other similar methods. Fourth, the MIMO cooperative spectrum sensing technique can also identify 5G signal with good performance and high data rate. Fifth, it showed a lower complexity versus other techniques as it employs a filter by taking into consideration on the real rates. This filter aided in removing the null bases as well as reduce the sensing times. Finally, it helps build a real-time spectrum sensing system, to enable hybrid filter detection of a 2×2 MIMO F-OFDM signal via simulation as well as mathematically. The simulation employs MATLAB, as well as compares the practical perfor-

mance pertaining to a 2 × 2 MIMO F-OFDM signal-based spectrum that can sense modules in GNU Radio Companion, applied on testbed based on National Instruments (NI) universal software radio peripheral with reconfigurable input/output (USRP N210) platform, by employing GNU Radio Companion.

4. Proposed cooperative spectrum sensing (CSS) based 5G environment model

Energy Detection can be defined as a simple detection technique employed for developing a blind signal detector since it can it overlook the signal structure. Energy detection follows the rule that computation of the detected signal energy can be done at the receiving end. It gives an estimation pertaining to the presence of a signal by performing a comparison of the energy received versus a known threshold γ that has been derived from the noise statistics. In short, the idleness case means that the band has noise only, while the busyness case means that the band has noise and traffic [29]. Thus, each hypothesis can be deduced from the rate of its error as described below:

$$\text{Pf} = \text{P (Decision} = \text{H1/H2)} \tag{1}$$

$$\text{Pmd} = \text{P (Decision} = \text{Ho/ H1)} \tag{2}$$

Where Pf is the false alarm probability, (also known as type I error) in spectrum sensing is the probability of incorrectly detecting a signal when there is no signal present in the spectrum. It is an important metric of the accuracy of spectrum sensing techniques, Pmd is the probability of missing a signal during spectrum sensing. It is defined as the ratio of the number of false negatives to the total number of samples. It is an important parameter in cognitive radio networks, as it determines the accuracy and reliability of the spectrum sensing process. If Pmd is too high, then the network may miss out on important signals, leading to degraded performance. The value of Pmd can be affected by several factors, such as the noise level, the signal-to-noise ratio, the bandwidth of the signal, and the sensing algorithm used. In order to reduce Pmd, it is important for cognitive radio networks to use more reliable sensing algorithms, reduce the noise level, and increase the signal-to-noise ratio, so Pmd + Pd = 1. The signal's energy is calculated based on Equation (3). This is carried out via calculation of the test statistics B followed by a comparison with the predefined threshold, i.e.:

$$\text{B} = 1/\text{N} \sum_{n-1}^{N} w(n)^2 \tag{3}$$

where B is the output of the energy detector, w[n] is the complex digitized signal, and N is the number of bins used.

In the absence of the primary signal, a central chi square distribution possessing N degrees of freedom is present for the decision statistic. Similarly, the decision statistic possesses a non-central chi square distribution with the same degrees of freedom in the presence of the primary signal [30]. If there is a large enough number of samples employed for detection (N > 250), Central Limit Theorem can be employed to approximate the distribution pertaining to the test statistic as Gaussian, along with mean and variance as stated in (4) pertaining to each of the hypotheses, in which σ_O^2 2 represents the variance with regards to the noise process and σ_s^2.

$$B - N\left(N\sigma_o^2, 2N\sigma_o^4\right) under\ H0 \tag{4}$$

$$B - N\left(N\left(\sigma_0^2 + \sigma_o^2\right)\right), 2N\left(\left(\sigma_0^2 + \sigma_o^2\right)2\right) under\ H1 \tag{5}$$

Two types of errors can be made when testing H0 compared with H1: either H0 or H1 can be falsely rejected. The first error is defined as a False Alarm, while the second one as a misdetection [31]. The probability of occurrence pertaining to both types of errors can be leveraged to measure the performance of energy detector, i.e., the probability of false alarm (PFa) [32], defining the probability pertaining to erroneously deciding the band to be occupied, even when it is not, and the probability of misdetection (PMD) can lead to erroneously deciding that the primary user is absent, when it is not the case. Another form that is employed for defining the performance is via complementation of the probability pertaining to misdetection, which is the probability of detection (PD) [33,31]. The rest of this research work has regarded PD in place of PMD to define the performance. PD and PFA can be statistically defined as:

$$PFA = Pr(B > \lambda D; H0) \tag{6}$$

The expression for PFA was derived from the definition of a false alarm, which is the probability of a false positive result given that the null hypothesis (H0) is true. In this case, the null hypothesis is that the two populations are equal, so PFA is the probability that the test statistic (B) is greater than the critical value (λD) given that the null hypothesis is true.

$$\text{PD} = \text{Pr}\,(\,\text{B} > \lambda\text{D};\ \text{H1}) \tag{7}$$

The probability PD is derived from the cumulative distribution function (CDF) of the random variable B. The CDF of B can be written as P(B ≤ λD), which is the same as 1-P(B > λ D). This means that the probability PD can be written as 1-P (B > λD) under the assumption of the null hypothesis H1.

Where B signifies the test statistic as defined by (2), while λ_D is the threshold that is regarded for determining the presence pertaining to primary users. Since B can also be approximately Gaussian distributed, assessment of the PFA and PD can be done as:

The derivation of the probability of a false positive (P_f) is based on the Neyman-Pearson lemma. The lemma states that the most powerful test of a given size is the one with the largest likelihood ratio.

The likelihood ratio is defined as the ratio of the probability of the data given hypothesis 1 (H1) versus the probability of the data given hypothesis 0 (H0). Pf = Prob{(H_1\H_0)} = L(H_1)/L(H_0) For a given sample size N and standard deviation σ_O, the likelihood ratio can be simplified to L(H_1)/L (H_0) = exp[(η-σ_Oˆ2)/(2σ_Oˆ2/N)].

Using the Q-function, we can then express the false positive probability as.

$$P_f = Prob\{(H_1\{H_0)\} = Q\left(\frac{\eta - \sigma_O^2}{\sqrt{\frac{2}{N}}\sigma_O^2}\right) \tag{8}$$

$$P_d = Prob\{(H_0\{H_1)\} = Q\left(\frac{\eta - \left(\sigma_O^2 + \sigma_s^2\right)}{\sqrt{\frac{2}{N}}\left(\sigma_O^2 + \sigma_s^2\right)}\right) \tag{9}$$

The above equation is derived from the cumulative distribution function of the ratio of two independent normally distributed random variables. The numerator of the ratio is the difference between the signal of interest (η) and the sum of noise variance (σ_Oˆ2) and signal variance (σ_sˆ2). The denominator of the ratio is the square root of the sum of (2/N) and the sum of the noise and signal variances. By applying the cumulative distribution function to the ratio of these two variables, we can calculate the probability of rejecting the null hypothesis (i.e., that there is no difference between the signal and noise variances).

Where Q () represents the Gaussian Q-Function. The design pertaining to a test for H0 compared with H1 includes a trade-off between the PD and PFA, since any decrease in the PFA can also result in decrease of the PD, while any increase in the PD can lead to increment in the PFA. The Neyman-Pearson criterion with regards to this trade-off includes placing a bound on the PFA as well as to enhance the detection probability in this constraint [31]. This criterion is sometimes also termed as Constant False Alarm Rate (CFAR). In this research paper, this approach has been used for threshold selection as well as to assess the detection performance via simulations. The threshold is attained from (5) as:

The expression for the detection threshold λD was derived by solving a Neyman-Pearson hypothesis test problem, which is used to determine the optimal threshold for a given false alarm rate (PFA) and signal-to-noise ratio (SNR). The threshold is defined as the value of the test statistic for which the probability of false alarm (PFA) is maximized. The expression for the threshold is derived by solving the following equation: PFA = Q-1 (λD - σ_Oˆ2)$\sqrt{2N}$ + N. Where Q is the cumulative distribution function of the test statistic, σ_Oˆ2 is the variance of the noise, N is the number of independent samples, and λD is the threshold. Solving for λD yields the expression:

$$\lambda D = \boldsymbol{\sigma}_O^2\left(\boldsymbol{Q} - 1(PFA)\sqrt{2\boldsymbol{N}} + N\right) \tag{10}$$

techniques to decide between the two hypotheses H0 and H1. The detector output, also called the test statistic, is then compared to a threshold in order to make the sensing decision about the PU signal presence. The sensing decision is performed as:

$$\boldsymbol{ifB} \geq \lambda \boldsymbol{H}1 \tag{12}$$

$$\boldsymbol{ifB} \geq \lambda \boldsymbol{Ho} \tag{13}$$

The sensing decision is derived by comparing the received signal strength (B) to a threshold (λ). If the received signal strength is greater than or equal to the threshold, then the decision is to accept the hypothesis (H1). If the received signal strength is less than the threshold, then the decision is to reject the hypothesis (Ho).

Where λ denotes the fixed threshold, which is impacted by noise; $PSDt$ represents overall PSD, and is also known as the decision static in binary hypothesis. Periodogram and radiometry are two alternative names for widespread and straightforward spectrum detection techniques adopted due to low complexity and computational needs [33]. There is no need for prior data concerning the PU waveform. The sensed signal's energy is evaluated and contrasted against the limit to validate if the spectrum is available for a secondary user [33]. It is possible to compute the energy detector decision statistic using the average of the squared values of Fast Fourier Transform (FFT) over N observations concerning the received SU waveform [34].

The ED methodology is implemented using frequency or time domain detection approaches. The former is superior because it monitors wider bands. Raw frequency domain monitoring is employed with Fast Fourier Transform (FFT) for determining PSD [35]. The signal received from the PU is split into overlapping parts that are transformed by the detector into the frequency domain using Fast Fourier Transform. The figure indicates the characteristics of the received waveform (only noise or a combination of signal and noise); the specified threshold is then determined. Subsequently, the signal is split into L overlapping parts, each having M simples. FFT and squared values are computed for every simple constituting the segments; then, a PSD is determined for every windowed portion, while the overall PSD averages help determine the test statistic. Lastly, the computed threshold is contrasted, and the decision concerning the presence of the signal is made using comparisons.

Cooperative spectrum detection critically relies on the decision mechanism during the second part. Detection information is collated from several cognitive relays, and fusion is employed with many results to arrive at a conclusion. The basic presumption regarding the binary-outcome spectrum sensing detection is [36,37]:

$$w(t) = \begin{cases} O(t) & : H_0 \\ S(t) + O(t) & : H_1 \end{cases} \tag{14}$$

Where $O(t)$ and $S(t)$ indicate the transmitted noise and signal. H_0 and H_1 denote the null and alternate hypotheses. Primary to secondary signal transmission allows secondary users to use spectrum detection. Each SU broadcasts a detection result bit to the centre, which uses decision fusion to account for all results provided by the users. A voting technique based on the OR rule is used to establish the presence of a primary user. This work uses user-based P_d and P_f values since sensing areas are not the same. The probabilities are computed as in eequation (8, 9). The Receiver Operating Characteristic (ROC) indicates the detection efficacy, suggesting the detection likelihood in contrast with the false alarm likelihood. ROC numbers are appropriate for superior detection likelihood and lower false alarms. This section is based on ROC for overall false alarm and detection probabilities. The following expression is used with regards to decision fusion based on the OR approach for M secondary users.

$$Q_f = 1 - \prod_{m=1}^{M}(1 - P_f) \tag{15}$$

$$Q_d = 1 - \prod_{m=1}^{M}(1 - P_d) \tag{16}$$

Where Q_f and Q_d denote the global probability values for false alarm and detection.

OFDM has been employed for wireless and wired broadband standards for over a decade. Presently, a broad category of discrete multi-tone transmission (DMT) recommendations like digital video broadcasting cable (DVB-C) and asymmetric digital subscriber line (ADSL) rely on OFDM. Moreover, wireless standards like IEEE 802.11, IEEE 802.16, LTE-advanced, and 5G use OFDM. The benefits concerning

orthogonality, closely packed orthogonal users help divide the available bandwidth among a narrow set of users. Moreover, it is feasible to use adaptive modulation techniques for subcarrier bands to enhance system bandwidth efficiency. The easy-to-implement OFDM approach affords high data throughput and flexible multi-path fading.

The transmission bandwidth is divided up into a collection of orthogonal subcarriers by OFDM. A general OFDM signal could be depicted as follows:

$$s(t) = \sum_{n=-\infty}^{\infty} s_n(t - nT) \tag{17}$$

Here, T stands for the length of an OFDM symbol, and $s_n(t)$ stands for the n-th OFDM symbol associated with a downlink slot, which can be depicted as:

$$s_n(t) = \sum_{k=0}^{K-1} a_{n,k}\delta(t) \otimes v(t) e^{j2\pi k\Delta ft} = \sum_{k=0}^{K-1} a_{n,k} v(t) e^{j2\pi k\Delta ft} \tag{18}$$

Here, $\delta(t)$ signifies the Dirac delta impulse, k specifies the number of subcarriers, k refers to the subcarrier index, $v(t)$ indicates the pulse shape (or prototype filter), Δf signifies the subcarrier spacing, and $a_{n,k}$ indicates the complex data symbol regarding the kth subcarrier and nth OFDM symbol. Regarding the traditional OFDM, the pulse shape $v(t)$ can be termed as a rectangular pulse with width T. Equations (1) and (2) can therefore be used to obtain the OFDM signal in the manner shown below [38]:

$s(t) = \sum_{n=-\infty}^{\infty} s_n(t - nT) =$
$\sum_{n=-\infty}^{\infty} \sum_{k=0}^{K-1} a_{n,k} v(t - nT) e^{j2\pi k\Delta f(t-nT)}$(19).

F-OFDM has emerged as a leading choice for the waveform used in 5G communication systems, as depicted in Fig. 1. F-OFDM continues to use OFDM as its primary waveform and sub-band filters for each sub-band with more than one subcarrier. Assuming that the spectrum shaping filter $h(t)$ is applied to the full passband for unified expression, there is only one sub-band in total [39].

$$s(t) = \sum_{n=-\infty}^{\infty} \left\{ \left[\sum_{k=0}^{K-1} a_{n,k} e^{j2\pi k\Delta f(t-nT)} \right] \otimes h(t - nT) \right\} \tag{20}$$

The F-OFDM transmitter block diagram illustrates the various components used to convert a serial data stream into a signal for transmission. The data is first converted from serial to parallel, which is the process of breaking down a continuous data stream into multiple parts. the IFFT is used to convert the frequency-domain data into the time-domain, and the parallel-to-serial converter is used to convert the parallel streams back into a serial stream. Next, a Cyclic Prefix (CP) is added to the parallel data stream, which is used to reduce interference from one symbol to the next. The CP is then followed by a Prototype Filter (g0[I]) to shape the signal in order to reduce spectral regrowth. After this, the signal is summed up, converting it back to a serial data stream. Finally, the serial data stream is transmitted as the F-OFDM signal.

5. The proposed model of 5G environment

The study and investigation of wireless access technology called as Multiple-Input Multiple-Output (MIMO) has been prompted by the lack of available bandwidth for wireless communication worldwide. It is a crucial technology that empowers next-generation networks by combining antennas at the transmitter and receiver to give exceptional spectrum and energy efficacy with comparatively simple processing [40]. Because of its greater spectrum utilisation and link dependability, the MIMO technology has emerged as one of the foundational components of 5G communication systems. Notably, as the MIMO system's antenna count rises, signal detection would have to contend with a challenge of high computing complexity and an inability to identify signals with low SNR. In view of this, this study suggests a 5G MIMO signal detection technique based on (HFD). [17]. As shown in Fig. 2, multi-user MIMO (MU-MIMO) is a group of multiple-input and multiple-output (MIMO) wireless communication technologies that enable communication between a number of users or wireless terminals, each of which has one or more antennas, on a single 2.4 GHz spectrum channel.

6. Proposed mathematical model

In this study, a hybrid filter is used in the CSS method to account for future 5G waveforms, as shown in Fig. 6 of this section. According to the equations below, the filter employed in this work processes the 5G waveform by utilising a cosine filter to execute energy monitoring using an SS frequency domain technique. The cosine filter is used to process the signal [41,42]:

$$R[0] = \frac{\sqrt{2}}{V} \sum_{v=0}^{V-1} r[v], \quad k = 0 \tag{21}$$

$$R[k] = \frac{2}{V} \sum_{v=0}^{V-1} r[v] \cos\left(\frac{\pi k(2v+1)}{2V}\right), \quad 1 \le k \le K-1 \tag{22}$$

where, $r[v]$ denotes the 5G waveform corresponding to length V. It is specified below:

$$r[v] = \begin{cases} O[v] & \\ S_{F-OFDM}[v] + O[v] & H_1 \end{cases} \quad v = 1, 2 \cdots, V \tag{23}$$

where $O[v]$ stands for Gaussian noise with a variance of $\sigma_O{}^2$ and a zero mean. The 5G signals that were received belonged to the $s_{F\text{-}OFDM}$ type, which is notable. Additionally, it was assumed that the signals were independent and that they utilised identically distributed (i.i.d) random approach with a zero mean and $\sigma_s{}^2$ variance. $R[k]$ represents the filtered signal corresponding to $r[v]$.

After the implementation of the cosine filter, Y'[k] was separated into nseg segments, with a lseg length, derived by way of the Welsh segmentation algorithm.

The algorithm works by first assigning a weight to each character in the string. The weights are assigned based on the frequency of occurrence of each character in the string. The algorithm then uses these weights to determine the optimal segmentation of the string into substrings of equal length.

This was followed by the computation of the PSD, for each segment, after they were individually windowed, with the utilization of the Hann window, is a technique used in signal processing to reduce or eliminate distortion caused by abrupt changes in the signal. It is a type of window function that is used to shape the edges of a signal in order to reduce spectral leakage. The window is applied to the signal before it is Fourier transformed in order to reduce the effects of spectral leakage. The window is also applied to the signal after the Fourier

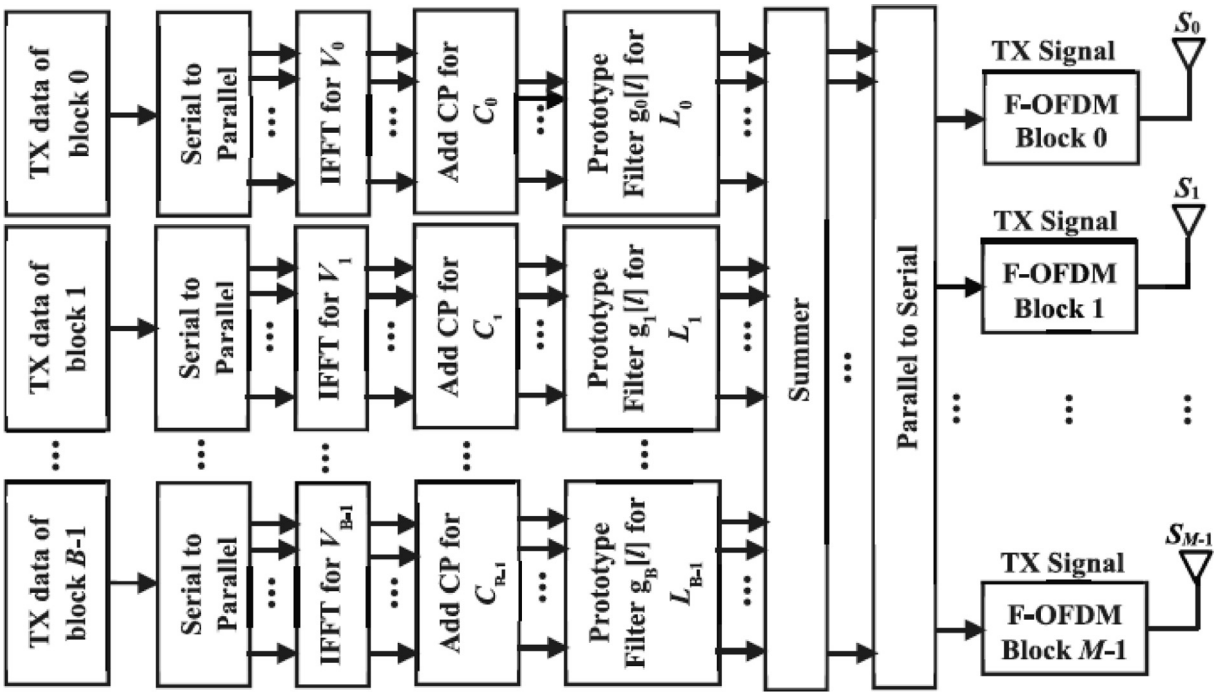

Fig. 1 F-OFDM transmitter Block Diagram.

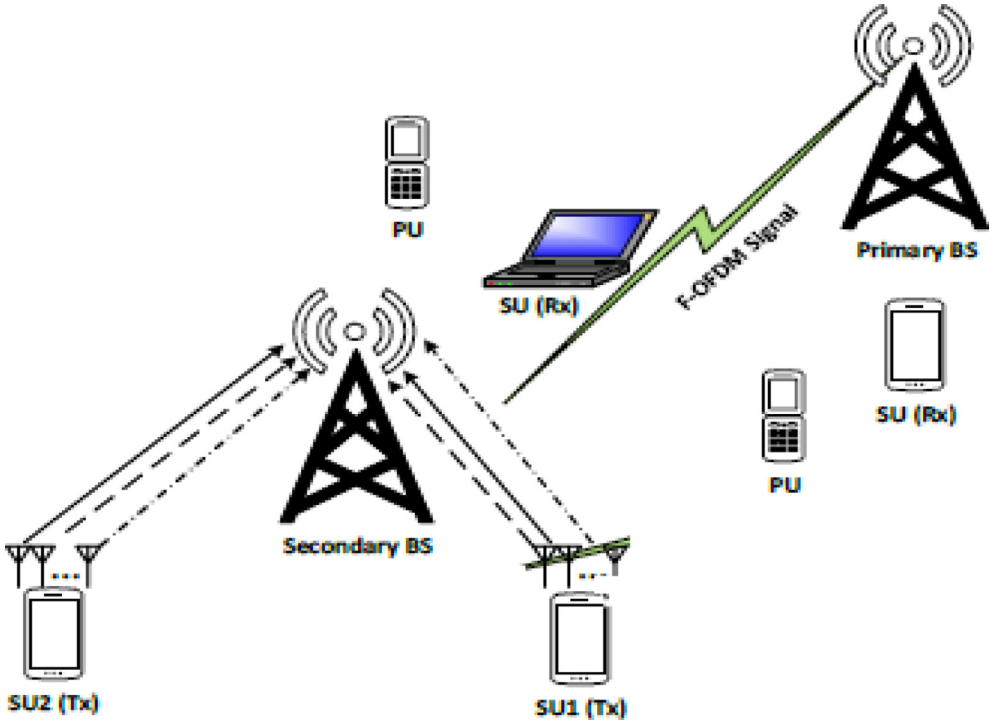

Fig. 2 model of MIMO Multi-user waveform CR-F-OFDM.

transform in order to reduce the effects of spectral aliasing. The Hamming window is a type of window that is used in signal processing and is defined by the equation:

$$w(n) = 0.54–0.46\cos(2\pi n/N).$$

where N is the length of the window.

The Hamming window is a type of window that is used to limit the effects of spectral leakage and to reduce or eliminate distortion caused by abrupt changes in the signal. Eventually,

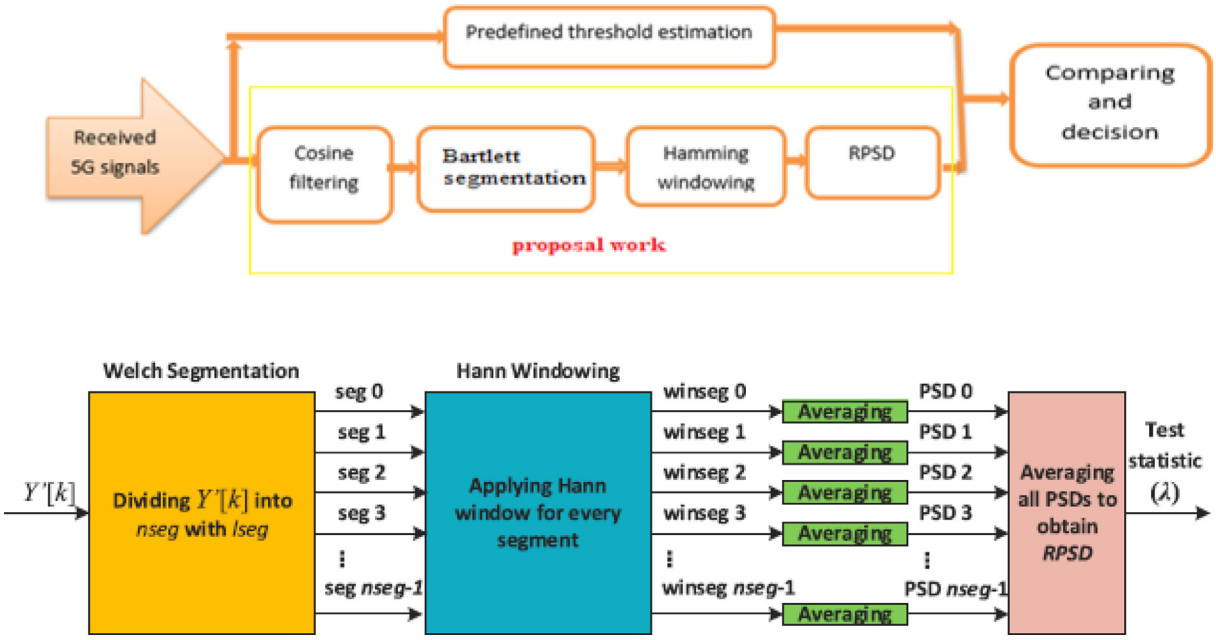

Fig. 3 The Proposed SS Technique for 5G Waveforms Block Diagram.

the consequential PSD (RPSD) was assumed the average of the previous PSDs. In the context of the decision statistic, this renders RPSD the regulating agent. This is portrayed in Fig. 3, where the expression 'seg' indicates segment, and 'winseg' indicates windowed segment.

The method that was suggested includes procedures like Hamming windowing, Bartlett segmenting, and cosine filtering (Fig. 3). The cosine filtering procedure separated the 5G waveform traffic from the Additive White Gaussian Noise (AWGN) channel noise. The Bartlett Segmenting step is then used to segment the filtered signals, reducing the noise variance. The third stage involved windowing each segment by utilising the Hamming windowing step to preserve the signal resolution. The technique attained the power spectral density and resultant for each windowed segment in the fourth step. The presence of the signal was then determined by comparing a test statistic (coming from the power spectral density) with predetermined standard threshold values. To attain smooth relationship, 1000 independent trials associated with the MC simulation for the various SNR rates are used to substantiate the mathematical model of the SS suggested system. The method's operations are restricted to the mean and only to real numbers, which reduces the complexity of the process. The cosine, for instance, comprises only the real bases by concentrating the signal on a small quantity of samples. They are real bases and they have lowered the number of samples. Be it Bartlett chart or Welch, it will simply split the new number into samples from tiny pieces, average each unit, then gather these rates to create one rate. It simply refers to adding and determining the rate. The windowing process is thus limited to creating a frame for every little piece and placing a Multiply in that window. Because there are no differentials, integrals, or natural logarithms, the arithmetic operations are quite straightforward. However, unlike Fourier, which deals with complex numbers, it only works with real numbers. The intricacy is therefore quite low.

The next stage is deleting the null coefficients that correspond to $R[k]$ to shorten sensing time by lowering computational requirements. Thus, K' is the updated $R[k]$ length, where $K' < K$ (i.e., $R'[k]$ is the $R[k]$ with K' length). For traffic movement, many samples are needed. After implementing the cosine filter, R' [k] was split into *Nseg* segments, with *Lseg* lengths, calculated by the Welch segmentation method. As a result, PSD values are calculated for each segment following isolation by utilising the Hamming window approach. Lastly, the overall PSD (*RPSD*), which is employed as the test statistic, is termed as the mean value of the earlier PSDs. For F-OFDM techniques, the earlier phases have been mathematically developed.

The cosine-filter processed F-OFDM signal is depicted in Eq. (24). Thus, Eq. (25) illustrates elimination of null coefficient.

The equation for F-OFDM can be derived from the Fourier transform of a periodic signal. The Fourier transform is used to represent a periodic signal as a sum of sinusoidal components, which can be expressed as:

F(k) = ∑_(v = 0)^(V-1)∑_(b = 0)^(B-1)∑_(m = 0)^(M−1)∑_(l = 0)^(L-1)∑_(n = 0)^(N-1)[s_(m,n)^b g_b [l]e^(j2πv ((n-l-mC))/N)].

where s_(m,n)^b is the modulation symbol of the b-th subcarrier in m-th OFDM symbol, g_b[l] is the channel gain of the b-th subcarrier at the l-th tap, and N is the number of subcarriers.

The Fourier transform of the periodic signal can then be expressed as:

F(k) = (-1)^k ∑_(v = 0)^(V-1)∑_(b = 0)^(B-1)∑_(m = 0)^(M−1)∑_(l = 0)^(L-1)∑_(n = 0)^(N-1)[(s_(m,n)^b g_b [l] e^(j2πv ((n-l-mc))/N))/√V +]Finally, the equation for F-OFDM can be derived by adding the cosine term to the Fourier transform:

$$R_{F-OFDM}[k] = (-1)^k \sum_{v=0}^{V-1} \sum_{b=0}^{B-1} \sum_{m=0}^{M-1} \sum_{l=0}^{L-1} \sum_{n=0}^{N-1} \frac{s_{m,n}^b g_b[l] e^{j2\pi v \frac{(n-l-mc)}{N}}}{\sqrt{V}} +$$

$$\sqrt{\frac{2}{V}} \sum_{v=0}^{V-1} \sum_{b=0}^{B-1} \sum_{m=0}^{M-1} \sum_{l=0}^{L-1} \sum_{n=0}^{N-1} s_{m,n}^b g_b[l] e^{j2\pi v \frac{(n-l-mC)}{N}}$$

$$\cos\left(\frac{\pi k(2v+1)}{2V}\right),\ 0 \le k \le K-1 \quad (24).$$

$$R'_{F-OFDM}[k] = R_{F-OFDM}[k] \quad ,\ 0 \le k \le K' - 1 \quad (25)$$

It is assumed that a $Ham[k]$ Hamming window operator (as depicted in Eq (26)) is used for each segment.

based on the Welch segmentation approach as specified ahead [29,30],

we taking the product of two cosine functions, namely: Ham[k] = 0.5 cos (0) + 0.5 cos(2πk/K) − 0.5 cos(πk/K) The first two terms (0.5 cos(0) + 0.5 cos(2πk/K)) form the cosine function with a period of 2πk/K, while the third term (0.5 cos(πk/K)) is the subtractive term which allows the window to be zero at both ends. Substituting 0.5 cos (0) = 0.54 and 0.5 cos(πk/K) = -0.46 into the equation gives the final result:

$$Ham[k] = 0.54 - 0.46\cos\left(\frac{2\pi k}{K}\right), \qquad 0 \le k \le K-1 \quad (26)$$

A PSD is obtained for every overlapped-windowed segmented,

$$PSD^{(j)}[k] = \frac{1}{L_{seg}} \left| \sum_{i=0}^{L_{seg}} R\prime[i] Ham[i] \right|^2,\ 0 \le k \le K-1, j = 1, 2, \cdots, N_{seg} \quad (27)$$

Here, R' denoted $R'_{F\text{-}OFDM}$, R'_{UFMC}, or R'_{FBMC}. The mean PSDs are assessed in the following manner:

$$RPSD = \frac{1}{N_{seg}} \sum_{i=0}^{N_{seg}-1} PSD(i) = \lambda \quad (28)$$

The equation above was derived by taking the sum of the power spectral density (PSD) values over all segments, and then dividing it by the number of segments. This gives an average PSD value, which is equal to λ.

Hence, the binary hypothesis for λ ($RPSD$) is:

$$\begin{cases} H_0, & \lambda \le B \\ H_1, & \lambda > B \end{cases} \quad (29)$$

Additionally, Eq. (8) is utilised to calculate P_f as it depends on the SNR and preliminary signal duration. Conversely, P_d is calculated using the revised length K'.

The formula for the probability of detection, P_d, is derived from the cumulative probability density function of the signal-to-noise ratio (SNR). Let K' denote the SNR threshold, and let σ_sˆ2 and σ_Oˆ2 denote the power of the signal and noise respectively. We also denote B to be the SNR of the received signal. Then the cumulative probability density function of the SNR is:

P(SNR ≤ B) = ϑ((B-K')/ (√ ((2/Kˆˆ)) ϑ((σ_sˆ2)/ (σ_Oˆ2) + 1))).

The probability of detection, P_d, is the probability that the SNR exceeds the threshold K', so it can be calculated as follows:

P_d = 1-P(SNR ≤ B) = 1-ϑ((B-K')/(√((2/Kˆˆ)) ϑ((σ_sˆ2)/ (σ_Oˆ2) + 1))).

Therefore, the formula for the probability of detection is:

$$P_d = Q\left(\frac{B - \vartheta\left(\frac{\sigma_s^2}{\sigma_O^2} + 1\right)}{\sqrt{\left(\frac{2}{K'}\right)\vartheta\left(\frac{\sigma_s^2}{\sigma_O^2} + 1\right)}}\right) \quad (30)$$

where.

$$\vartheta = \frac{K}{K'} \quad (31)$$

The system error (global probability of error) can be expressed as.

$$Q_e = 1 - Q_d + Q_f \quad (32)$$

The system error (global probability of error) is the sum of the probabilities of all individual errors, which is calculated by subtracting the probability of correct operation (Q_d) from the sum of the probabilities of all possible faults (Q_f). In other

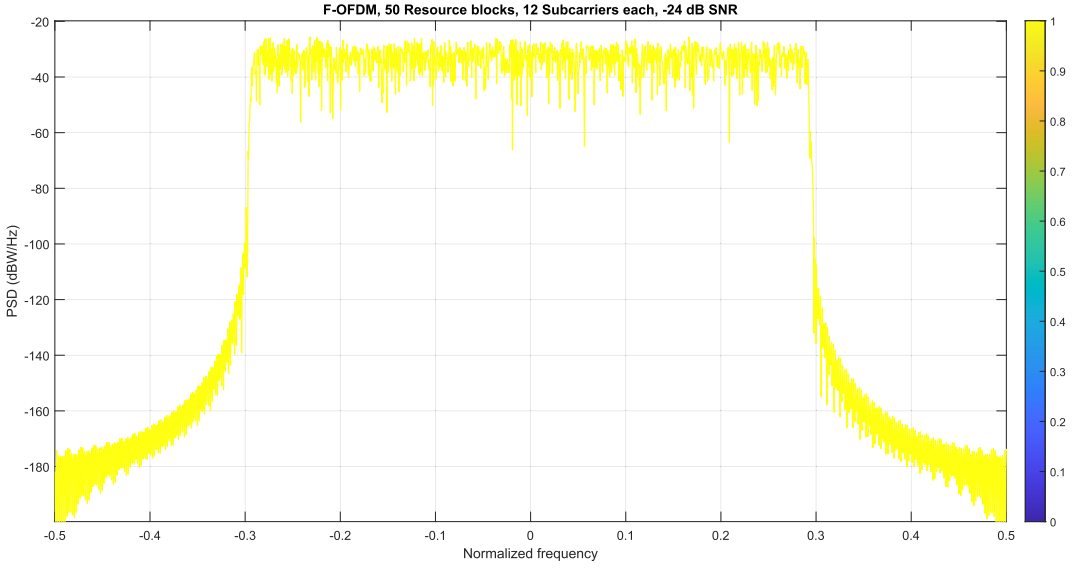

Fig. 4 The PSD of Received MIMO-F-OFDM for −24 dB SNR Value.

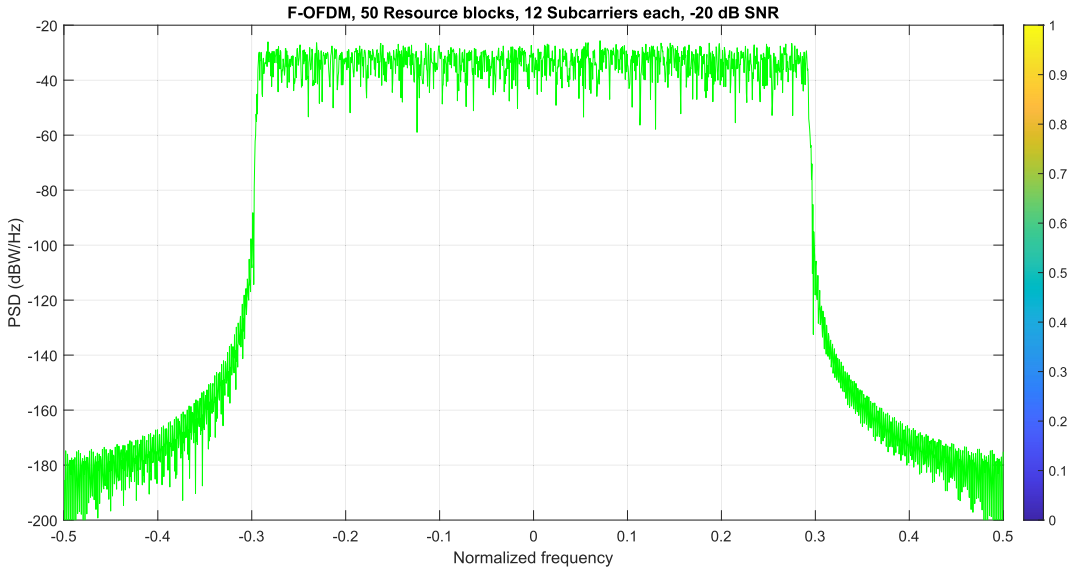

Fig. 5 The PSD of Received MIMO-F-OFDM for −20 dB SNR Value.

words, the system error (Q_e) is equal to 1 minus the probability of correct operation (Q_d) plus the probability of all possible faults (Q_f).

7. Impact of SNR on received signals

Here, several SNR rates have been used to display the resulting F-OFDM waveform that we generated before waveform detection by using mat lab 2020 and sent via platform USRP in section 6. They observed that the SNR had a substantial impact on the system's sensing ability, as the spectrum of the received F-OFDM waveform signal was impacted by SNR rates. Figs. 4, 5, and 6 depict the PSDs of obtained F-OFDM waveforms which were produced by utilising the SNR rates of (−24) dB, (−20) dB, and (−16) dB.

Fig. 7 displays the PSDs of received F-OFDM (which was mixed with all SNRs). Hence, the noise variance (which was mixed with the produced waveforms) for the (−24) dB SNR was the largest, while the noise variance for (−16) dB SNR was the lowest. As shown in the figure, the PSD of the received F-OFDM signal was high if noise variance was high. It follows that the received F-OFDM signal with (−16) dB SNR was the clearest, but those with (−20) and (−24) dB SNR were not. Thus, the traffic projection was impacted by the SNR rates and required a precise sensing technique. The recommended sensing approach tackled this issue entirely and could distinguish between the traffic and noise.

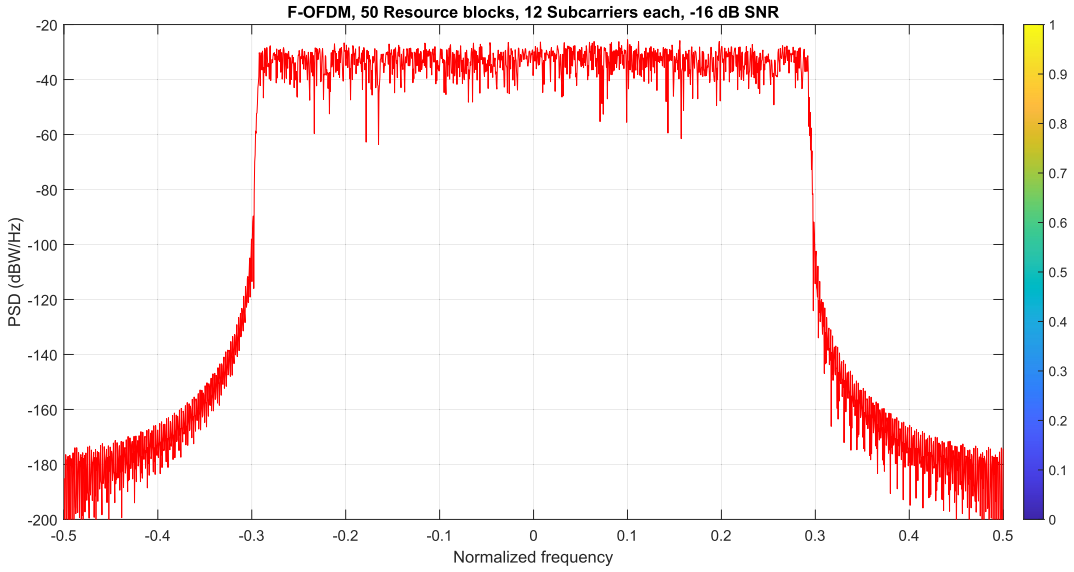

Fig. 6 The PSD of Received MIMO-F-OFDM for −16 dB SNR Value.

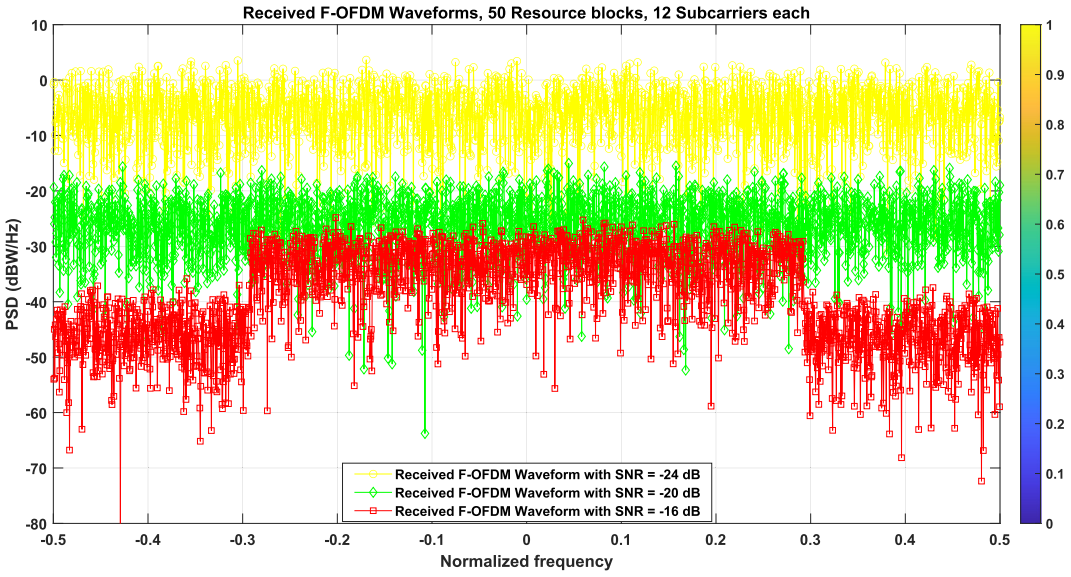

Fig. 7 The PSD of Received MIMO F-OFDM for Various SNR Values.

8. Implementation platform

The specified MIMO F-OFDM approach is tested using the National Instruments SDR USRP N210 system, as depicted in Fig. 8. This system operates in the 70–6 GHz range, allowing external PPS reference, 10 MHz external reference input, and 200 kHz – 56 MHz variable analogue bandwidth. MIMO is selected as the default technique when a compound multi_usrp is employed to create a multi-channel streamer. It suggests the samples across streams have automatic alignment. A PC is linked to the USRP using the 832 MB/s NI PXIe-PCIe8371 card. ADCs are used to amplify the IF baseband signals, followed by programming the digital versions on an FPGA. The stock FPGA snapshot offers digital down-conversion, allowing precise frequency tuning and multiple decimation filters. Decimation is followed by streaming raw and other data to a host system using its interface. The process is reversed to use the transmission side. Overall, the USRP facilitates straightforward prototyping of sophisticated signals in a frequency band that addresses the primary bandwidths in use for mobile communication systems.

Fig. 9 depicts the testbed used in the lab to implement the hybrid filter detection sensor. One personal computer (PC) is linked with two N 210 USRPs (USRP Tx and USRP Rx) having Vert900 antennas using three CAT6 Gigabit Ethernet (GbE) links having RJ45 connectors; a GbE switch connects

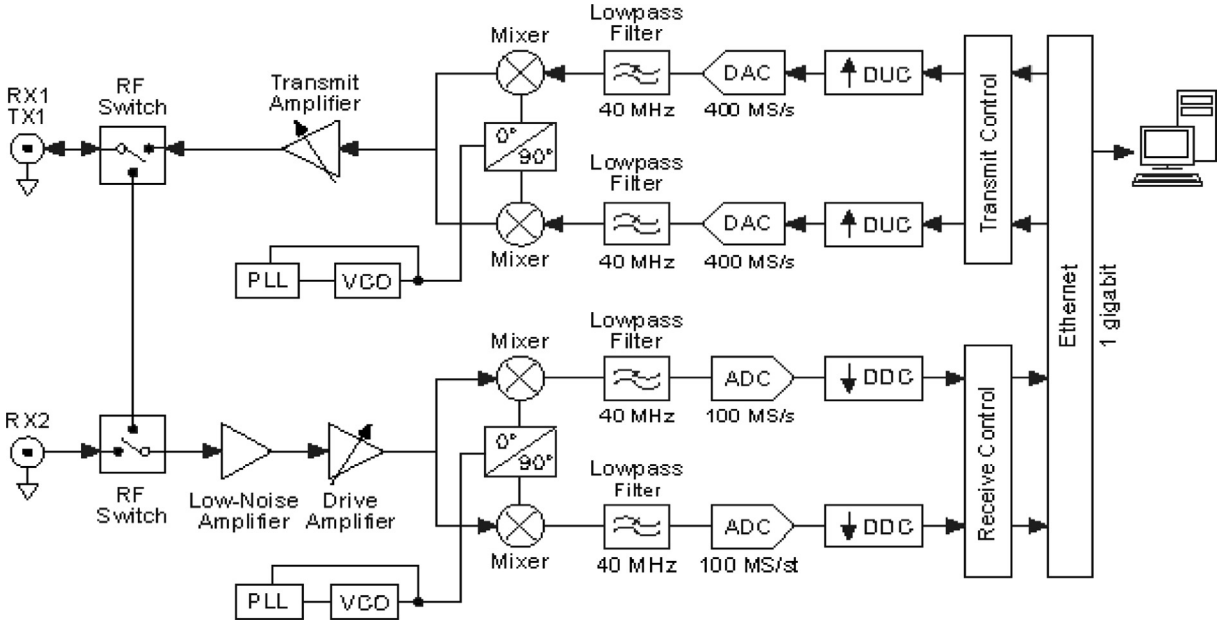

Fig. 8 Schematic Diagram of a Universal Software Radio Peripheral N210 [43].

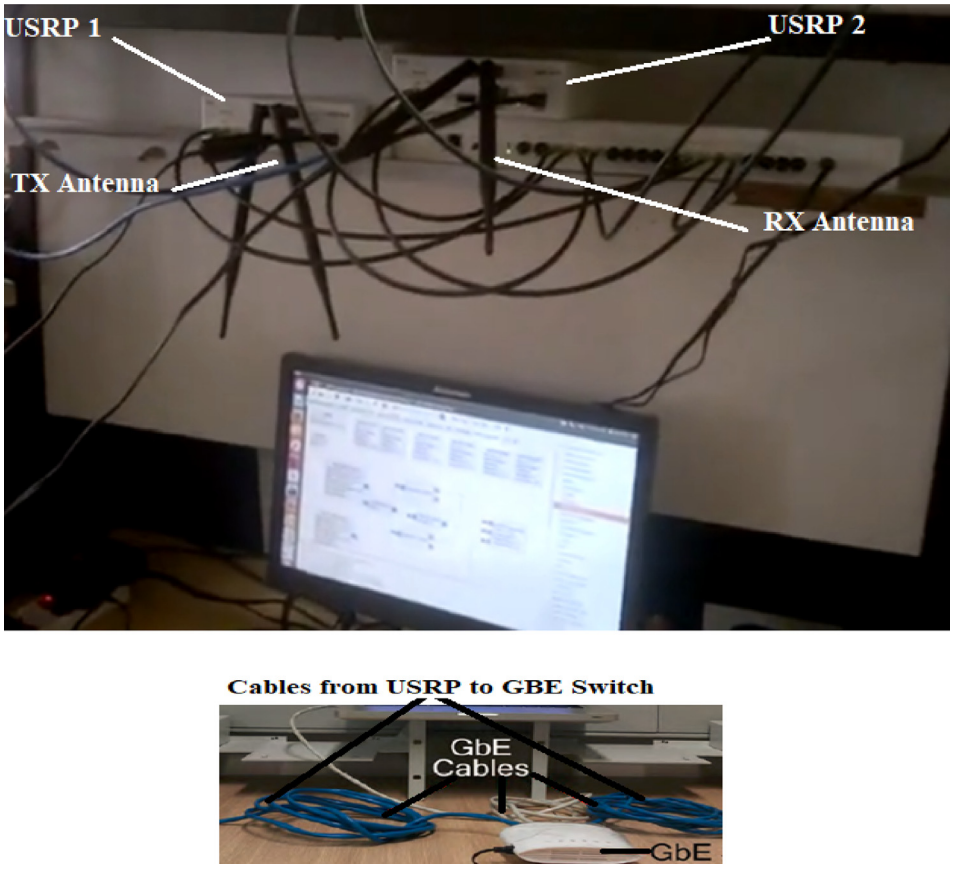

Fig. 9 Experimental Setup for Spectrum Sensing using GNU Radio and USRP.

these links. This research used GNU Radio v3.7.7 running on Mac OS.

As depicted in Fig. 9, the National Instruments (USRP) N 210 can be used to implement a 2x2 multiple-input multiple-output (MIMO) F-OFDM transceiver. The suggested technique uses the radio frequency technique and can be validated successfully for a 70 MHz to 6 GHz transceiver range. Moreover, it offers MIMO ability, and the typical F-OFDM system framework is available at the USRP. It suggests that present technology can process sophisticated signals. Fig. 10 depicts the data path from the Rx/Tx systems to the Central Processing Unit (CPU). The schematic diagram comprises orange arrows to depict reception and transmission links. The GRC portions produce an F-OFDM test waveform meant for the primary user based on the USRP transmitter (Tx). The USRP Rx behaves as the secondary consumer (cognitive radio) and constantly monitors the spectrum to detect primary users. The signal obtained by the secondary user is processed using hybrid filter detection (HFD) using GRC on the PC; the test statistic concerning energy is used for the conclusion. Typically, F-OFDM offers better outcomes because of an extended sample set. A short sensing period is vital because F-OFDM uses shorter streams.

MATLAB is high-level language-based software; version 2021 was employed to create the framework for the spectrum detection technique. The PU was devised using MATLAB, creating a Quadrature Amplitude Modulation based F-OFDM test waveform. AWGN is integrated with the created waveform, resulting in the waveform received by the SU. Subsequently, the energy test statistic is calculated and contrasted against a specified limit based on a particular false alarm likelihood. Detector accuracy is enhanced using 1000 Monte Carlo iterations. Table 1 lists the required aspects employed for this setup. The USRP1 transmitter uses FPGA, while the receiver uses USRP2 to collect the F-OFDM waveform.

9. Results and discussion

9.1. Simulation results

a. Detection Mutli- user MIMO F-OFDM under AWGN channel.

CSS implementation pertaining to the CRN-5G system is recommended to monitor the F-OFDM signal from a 5G network. MATLAB and MathWorks® were used to simulate the devised CSS system. The experiment comprised signal identification in challenging conditions, i.e., sub-zero SNR values, to evaluate the efficacy of the devised system. Further, one thousand Monte Carlo iterations were completed. Fig. 11 depicts signal strength (SNR = -24 dB to −16 dB) and detection likelihood for different sample sizes (256, 512, 1028, and 2048). The false alarm likelihood was 0.01.

The plot indicates higher detection probability as SNR decreases, suggesting that the signal is stronger at lower SNR. The likelihood of identifying a PU increases due to the use of hybrid filter detection.

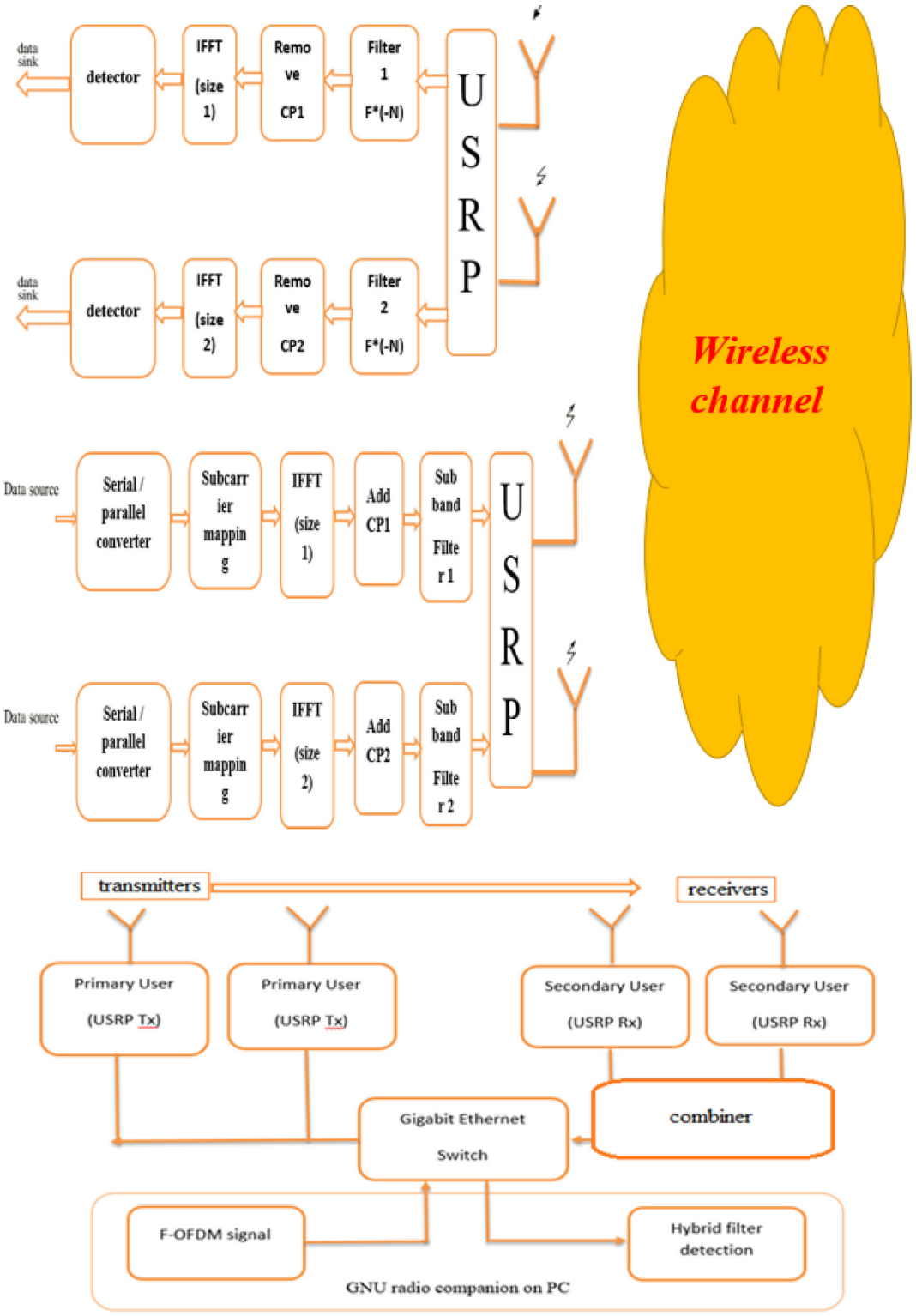

Fig. 10 Testbed Architecture Block Diagram (Block diagram of the implemented MIMO F-OFDM system).

Further, the computed outcomes indicated that hybrid filter detection helped obtain appreciable detection probability at low SNR; at the same time, false alarm likelihood was lower. The sensing efficacy (i.e., ROC) of the proposed approach for the received F-OFDM waveforms is depicted in Fig. 12. A comparison is made with conventional systems based on −24, −20, and −16 dB SNR values.

The conventional detection approach was selected for the frequency domain based on the Fast Fourier Transform (FFT). The proposed model of the devised system is validated

Table 1 Parameters of simulation and practical MIMO F-OFDM.

Parameters of simulation and practical MIMO F-OFDM
Number of FFT = 2048
Number of Resource Block = 50
Number of sub-carriers = 12
Length of cyclic prefix = 72
Bits / Sub-carrier = 6
Tone offset = 2.5
Length of filter = 513
Transmitter oversampling factor = 2
Carrier frequency = 2.4 GHz
Number of iterations = 1000
PU signal = F-OFDM
Channel noise = AWGN
Number of samples/ FFT size = 23,128, 256, 512, 1024, 2048
Signal-to-noise ratio = -30 dB to 0 dB
Probability of false alarm = 0 to 1
Desired probability of detection = 0.9
Desired probability of false alarm = 0.1
64 QAM
Number of sensing samples = 300

based on 1000 independent MC simulation iterations for different SNR values to predict an accurate correlation. Fig. 12 depicts ROC characteristics using pink, blue, and yellow to depict the traditional efficacy (ROC) at −24, −20, and 16 dB SNR, respectively. SNR was highest for the yellow line, indicating optimal performance; however, the detection rate was 0.033, and the false-alarm likelihood was 0.01. On the other hand, the proposed SS system ROC plot was designated as simulated or mathematical. These ROC plots depicted detection efficacy at −24, −20, and −16 dB SNR values. The detection likelihood values were 0.874, 0.886, and 0.892 at a 0.01 false-alarm likelihood for −24, −20, and −16 dB SNR values, respectively. ROC plots concerning the SS approach exhibited significantly better performance than legacy systems since SS dampened noise variance. Moreover, the mathematical model was validated using the MC as depicted in Fig. 12 for the ROC plot depicted using the suggested colour-symbol combinations for SNRs of (−24), (−20), and −16 dB, respectively. The ROC simulation also exhibited better detection likelihoods (0.873, 0.876, and 0.883) at a 0.01 false-alarm likelihood corresponding to −24, −20, and −16 dB SNR rates, respectively.

In case the probability of false-alarm equals 0.05, the depicted detection efficacy corresponds to (−24), (−20), and −16 dB SNR values, respectively. Detection likelihoods were (0.973, 0.985, 0.993) at a 0.05 false-alarm likelihood corresponding to (−24), (−20), and −16 dB SNR values, respectively. ROC plots concerning the SS approach exhibited significantly better performance than legacy systems since SS dampened noise variance. Moreover, the mathematical model was validated using the MC as depicted in Fig. 15 for the ROC plot depicted using the suggested colour-symbol combinations for SNRs of (−24), (−20), and −16 dB, respectively. The ROC simulation also exhibited better detection likelihoods (0.973, 0.977, and 0.983) at a 0.05 false-alarm likelihood corresponding to −24, −20, and −16 dB SNR rates, respectively. The mathematical and simulation models exhibited identical detection likelihoods. They were also superior to the traditional technique, as indicated in Table 2.

Simulation outcomes show that.

1) Higher detection likelihood for Hybrid Filter Detection (HFD) than ED.
2) The suggested Hybrid Filter Detection approach is superior to ED concerning its detection ability pertaining to a primary user using a licensed spectrum. False alarm likelihood was below 0.01. This usable hybrid filter is based on low SNR values (-24, −20, −16) dB corresponding to (256, 516, 1024, 2048) sample sizes.

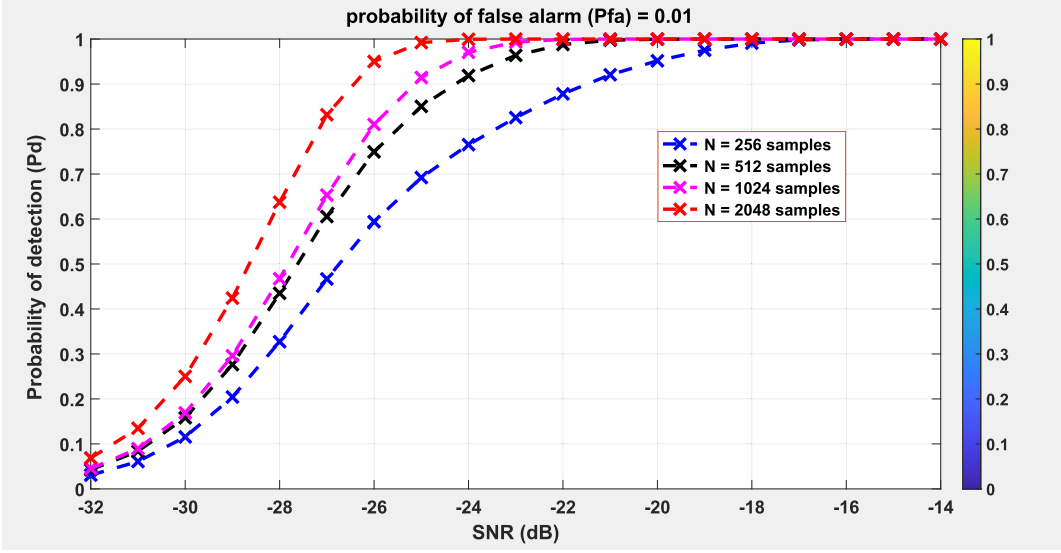

Fig. 11 Signal-to-noise ratio versus probability of detection with varying Sample Size (Pfa = 0.01, SU = 50) for MIMO F-OFDM under AWGN channel.

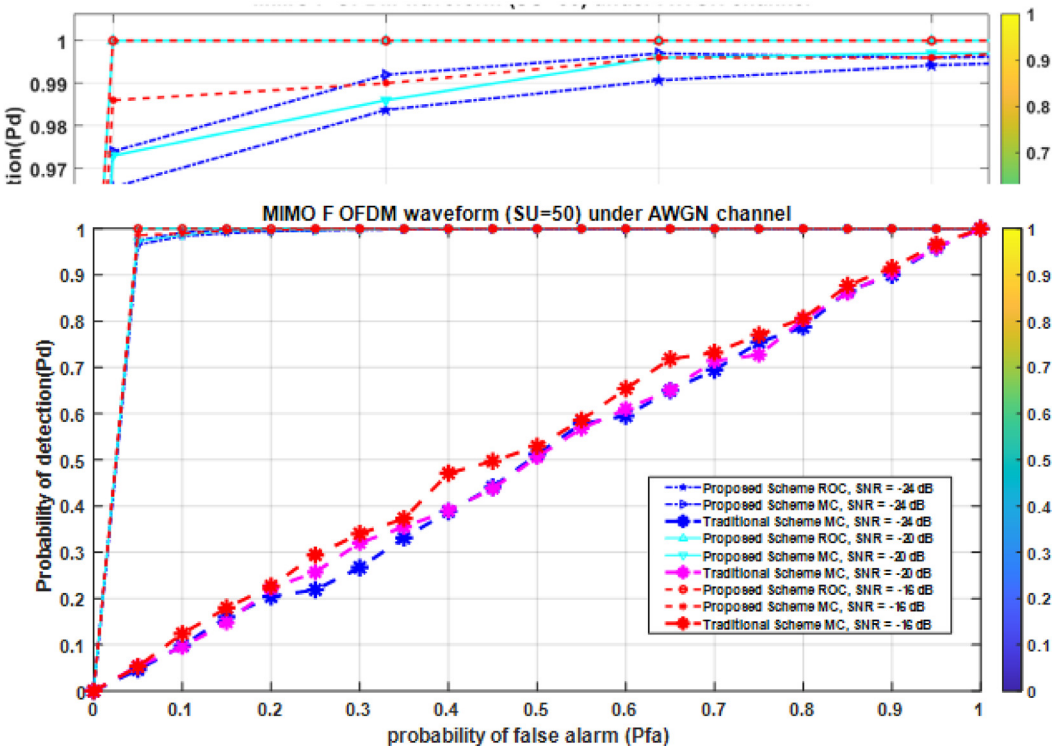

Fig. 12 The ROC of proposed system and traditional system for MIMO F OFDM waveform)SU = 50) under AWGN channel.

Table 2 comparison of detection probability (mathematical, simulation) of MIMO-F-OFDM (SU = 50) between false-alarm probability in the case of 0.01 and 0.05.

MIMO-F-OFDM	false-alarm probability = 0.05			false-alarm probability = 0.01		
	SNR = -24 dB	**SNR = -20 dB**	**SNR = -16 dB**	**SNR = -24 dB**	**SNR = -20 dB**	**SNR = − 16 dB**
detection probability (mathematical)	**0.973**	**0.985**	**0.993**	**0.874**	**0.886**	**0.892**
detection probability (simulation)	**0.973**	**0.977**	**0.983**	**0.873**	**0.876**	**0.883**
detection probability traditional	**0.56**	**0.55**	**0.55**	**0.013**	**0.012**	**0.01**

3) They asserted that the approach exhibited superior sensing ability than other comparable methods. The MIMO-F-OFDM signal had a 0.8 detection likelihood using the recommended approach; moreover, false alarm likelihood was below 0.01, corresponding to a less than 0 dB SNR with reduced computational complexity.
4) In contrast, the MIMO cooperative spectrum detection approach aims to identify different 5G waveforms at high throughput and acceptable performance. The outcomes from the real-world test of the hybrid filter detector based on USRP are highlighted. The plots based on real-time data have been verified; they indicate an aligning pattern similar to the Monte-Carlo simulations. We note that sensor efficacy can be enhanced by using a greater sample count since it can remove channel noise during test statistic computation, allowing better SNR. Moreover, the outcomes indicate that detection probability must be optimised to deliver high performance; conversely, false alarm likelihood must be reduced. Simulation comparison with real-time hybrid filter detection indicates that the experimental can identify signals with SNR values as low as −24 dB. Typically, the tested real-time hybrid filter detector had inferior outcomes that might be attributed to noise distribution not being precisely AWGN.

b. The impact of M−ary rates on MIMO F-OFDM signals detection

The 5G F-OFDM signal was modulated at different M−ary QAM rates. The sensing characteristics were determined for 10, 30, and 50 SUs at three SNR values, i.e. −16, −20, and −24 dB. The specified 5G signal and the proposed framework were implemented using MATLAB. The figures depicted below indicate characteristics for QAM, 16QAM, 64QAM, and 256QAM at −16 dB, −20 dB, and −24 dB SNRs. These titles are for the array variety QAM used for generating the F-OFDM signal.

A shorter stream was sensed for obtaining the data since the use case exhibits more noise variance compared to the previous

test. Though the second scenario has a lower SNR value, the overall detection likelihood is superior to the previous case because the recommended hybrid filter dampens effects on SNR while reducing the starting stream length. Similarly, Figs. 13, 14, and 15 indicate the performance corresponding to −24 dB SNR. The new sample count is 1522 based on the suggested hybrid filter, allowing superior performance than the first scenario. To improve the overall detection likelihood, noise variance is more than before, the stream is shortened further, and the SU count is enhanced. These are the most effective aspects, as depicted in the detection characteristics concerning the second and third scenarios.

The F-OFDM signal sensing performance is specified in Figs. 13, 14, and 15. Signal sensing performance is affected by M−ary QAM. Considering that the new waveform has the same length for all array varieties, detection efficacy is different based on array count. Array count impacts signal detection since a higher count increases the error rate among the symbols. The detection efficacy of the recommended approach for F-OFDM systems is higher since it has an extended signal stream. In contrast, the sensing efficacy of the recommended technique for 4-QAM signals is superior to 16-, 64-, and 256-QAM because it has the slightest bit rate among these. Moreover, this system senses better for 50 SUs using the specified

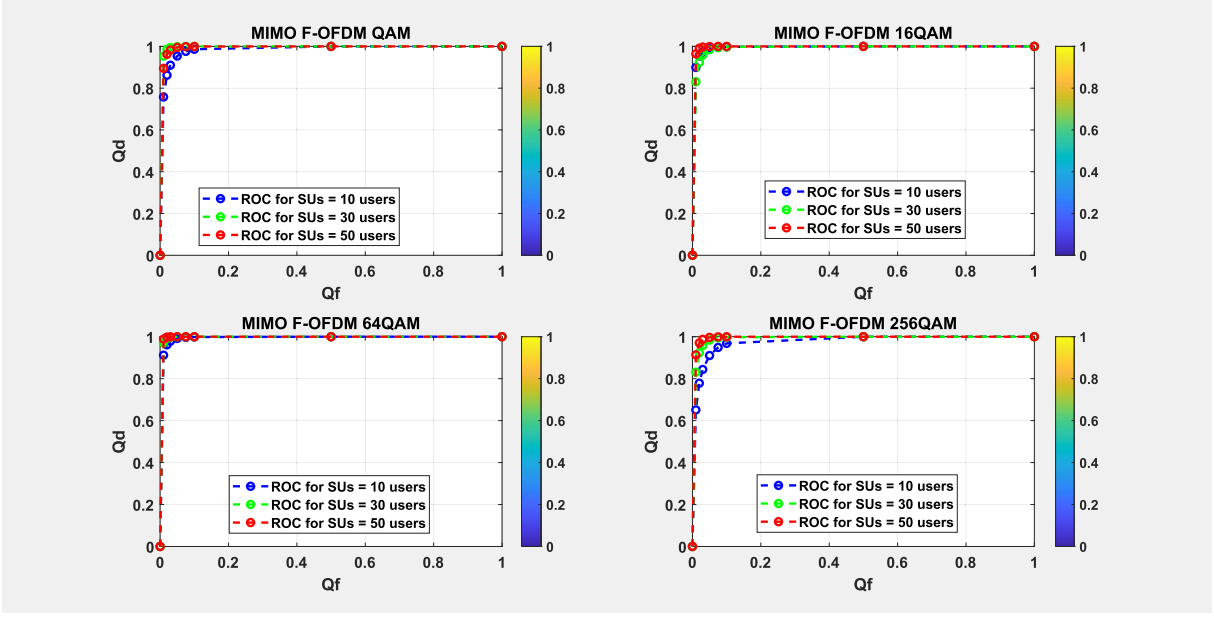

Fig. 13 MIMO- F-OFDM Sensing with SNR = -16 dB for (a) QAM, (b) 16QAM, (c) 64QAM, and (d) 256 QAM.

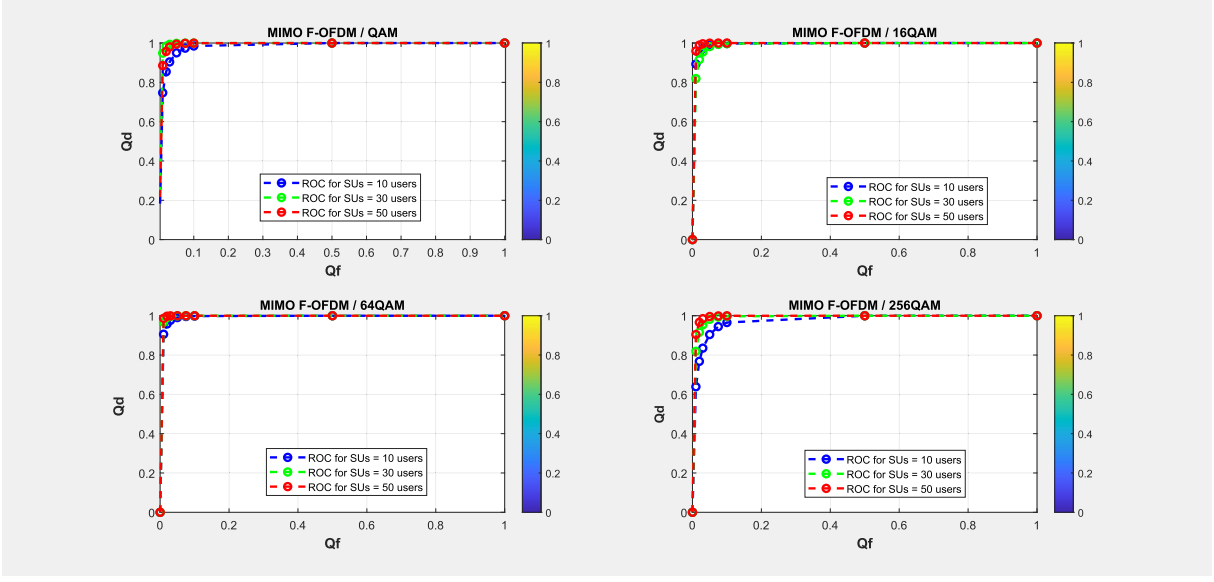

Fig. 14 MIMO- F-OFDM Sensing with SNR = -20 dB for (a) QAM, (b) 16QAM, (c) 64QAM, and (d) 256 QAM.

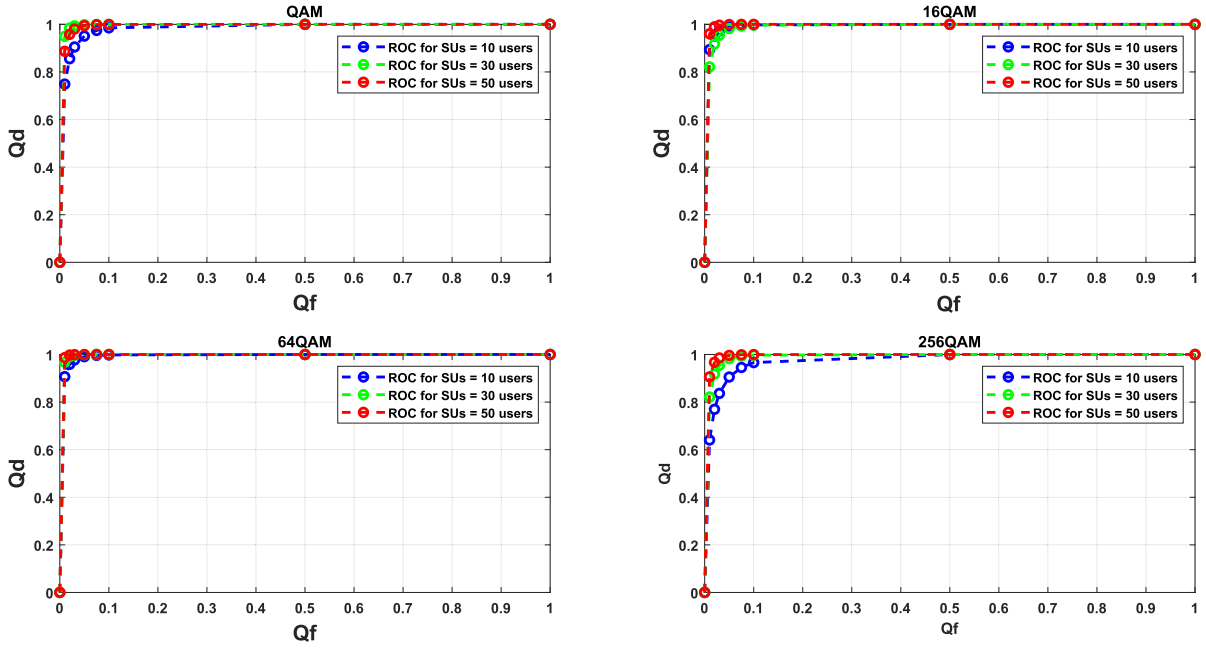

Fig. 15 MIMO-F-OFDM Sensing with SNR = -24 dB for (a) QAM, (b) 16QAM, (c) 64QAM, and (d) 256 QAM.

Table 3 *Qd* of F-OFDM-5G Waveform for Given *Qf*, SNR, and SUs Ratios.

SUs NO.	From Fig. 16 SNR = -16 dB	From Fig. 17 SNR = -20 dB	From Fig. 18 SNR = -24 dB
10	*Qd* = 0.9065	*Qd* = 0.9955	*Qd* = 0.981
20	*Qd* = 0.903	*Qd* = 0.9955	*Qd* = 0.973
50	*Qd* = 0.911	*Qd* = 0.9965	*Qd* = 0.979

waveform than 30 or 10 SUs because it's the most significant count, as highlighted in Table 3.

The new sample count is 1522 based on the recommended hybrid filter, which performs better than the first scenario. To improve the overall detection likelihood, higher noise variance levels are used, sensed stream length is reduced, and raising the SU count are understood as the critical aspects, as highlighted in the detection differentiation in the second and third scenarios.

c. The impact error of proposed system of 5G (MIMO F-OFDM) waveform

The information discussed in this section concerns reducing the error likelihood for Pfa = 0.01 and 0.05. The mathematical outcomes are appreciable and noteworthy concerning performance improvement regarding spectrum detection for cognitive radio networks.

Fig. 16 depicts the error likelihood for the suggested SS approach. All error likelihoods concerning the simulation and mathematical approaches were computed using Eq. (3). The plots indicate −24 dB, −20 dB, and −16 dB SNR, respectively. It was observed that two different colour curves depict a close error likelihood for the two methods. Considering a 0.05 false alarm likelihood, the error probabilities for −26, −20, and −16 dB were 0.0765, 0.0641, and 0.0589, respectively. Therefore, error likelihoods were reduced as SNR values increased. The recommended SS approach exhibited a suitable error rate likelihood of 0.0765 for a low SNR (-24 dB). In contrast, the error likelihood for the conventional methodology was more for the specified SNR values. Therefore, the recommended SS framework produced fewer errors, making signals more accurate.

d. The impact the global error probability of 5G (MIMO-F-OFDM) waveform

System error is critical to ascertain the effectiveness and accuracy of a devised detection technique. System error might be calculated using false alarms and missed detection likelihoods. Fig. 17 depicts the system error corresponding to the sensing abilities of the F-OFDM MIMO system. To offer enhanced detection abilities, overall false alarm likelihoods (Qf) must remain close to 0.01. The global error likelihood reduces as the SU count increases even at lower SNR values because the recommended hybrid filter reduces the effects of low SNR.

e. Impact MIMO F-OFDM (ED and HFD) techniques on AWGN and Rayleigh channel in M−QAM

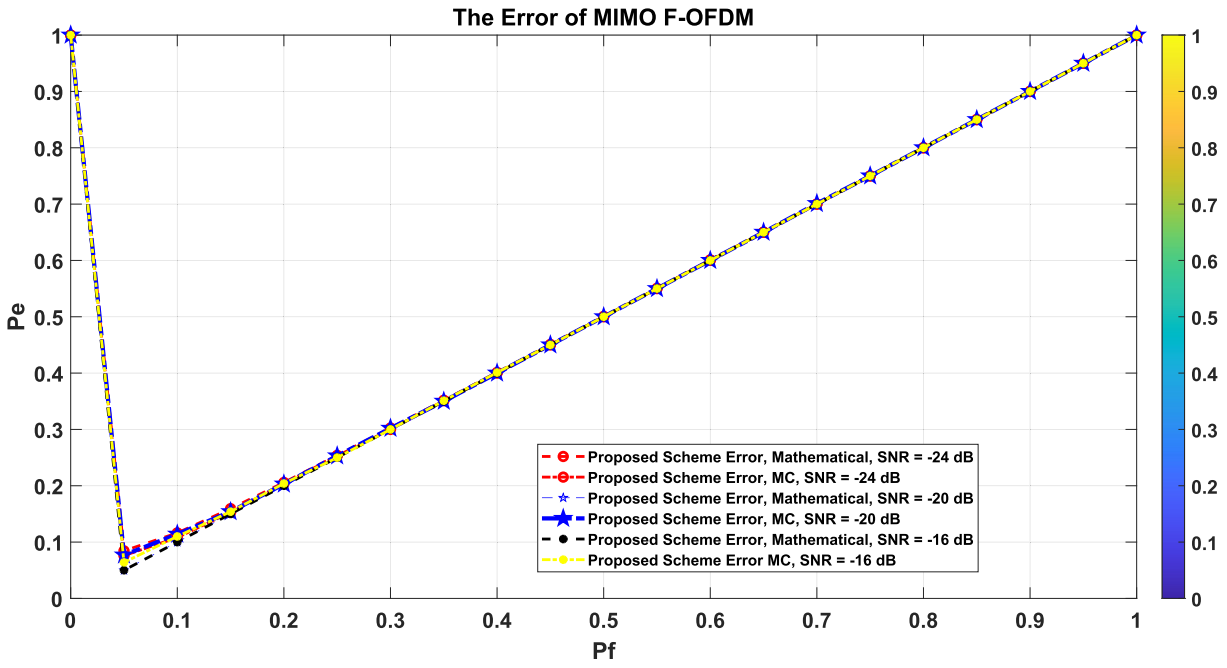

Fig. 16 The Error of Proposed System of 5G (MIMO F-OFDM) Waveform.

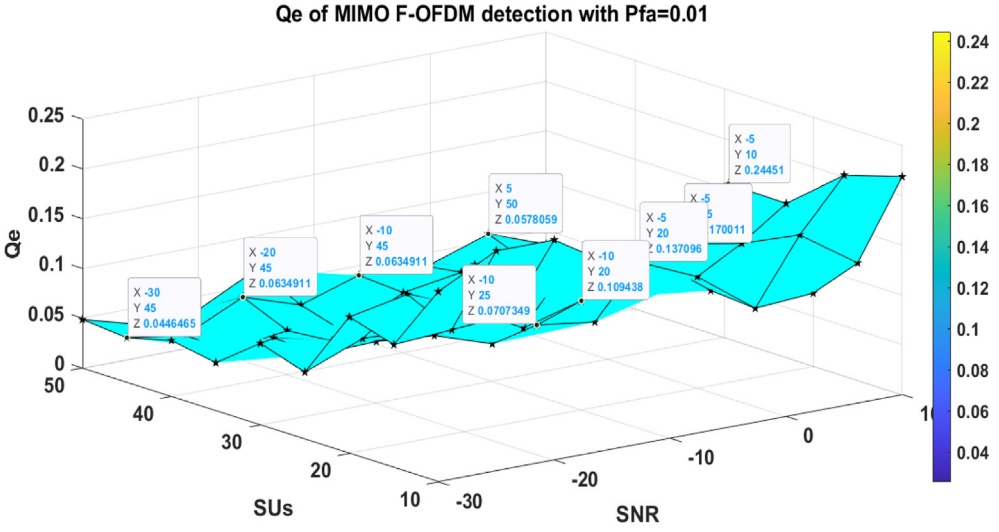

Fig. 17 Qe of MIMO- F-OFDM for Qf = 0.01.

This section discusses the aspects of MIMO F-OFDM system equivalence using M−QAM−based AWGN (additive White Gaussian Noise) and Rayleigh fading channels. The recommended HFD technique is contrasted against energy detection (ED) for two use cases: Rayleigh and AWGN channels, as depicted in Figs. 18, 19, 20, and 21. Algorithm effectiveness is gauged using receiver operating characteristics (ROC) plots, Pd and Pfa for specific SNR values.

Figs. 18 and 19 present the AWGN fading characteristics of HFD and ED methods for 0.01 Pfa. The figure indicates that the proposed technique is superior to ED concerning detection likelihood, specifically at low SNR, as shown in Fig. 18. The other benefit of this technique is that perfect detection likelihood was attained 11 dB before ED. For example, the suggested technique achieves PD = 0.9 at −27 dB SNR; ED reaches that number at −16 dB. Fig. 19 depicts this superior detection performance obtained 10 dB before ED. For example, the proposed technique obtains 0.9 PD at −24 dB SNR compared to −14 dB for ED.

Figs. 20 and 21 depict the assessment of the suggested HFD technique against ED for the Rayleigh fading scenario. Fig. 20 depicts that the suggested technique hit the detection likelihood threshold 4 dB before ED. The suggested technique achieves 0.9 PD at −26 dB compared to –22 dB for ED. Based on Fig. 21, the suggested technique achieves the required detection likelihood 6 dB before ED. For example, the suggested

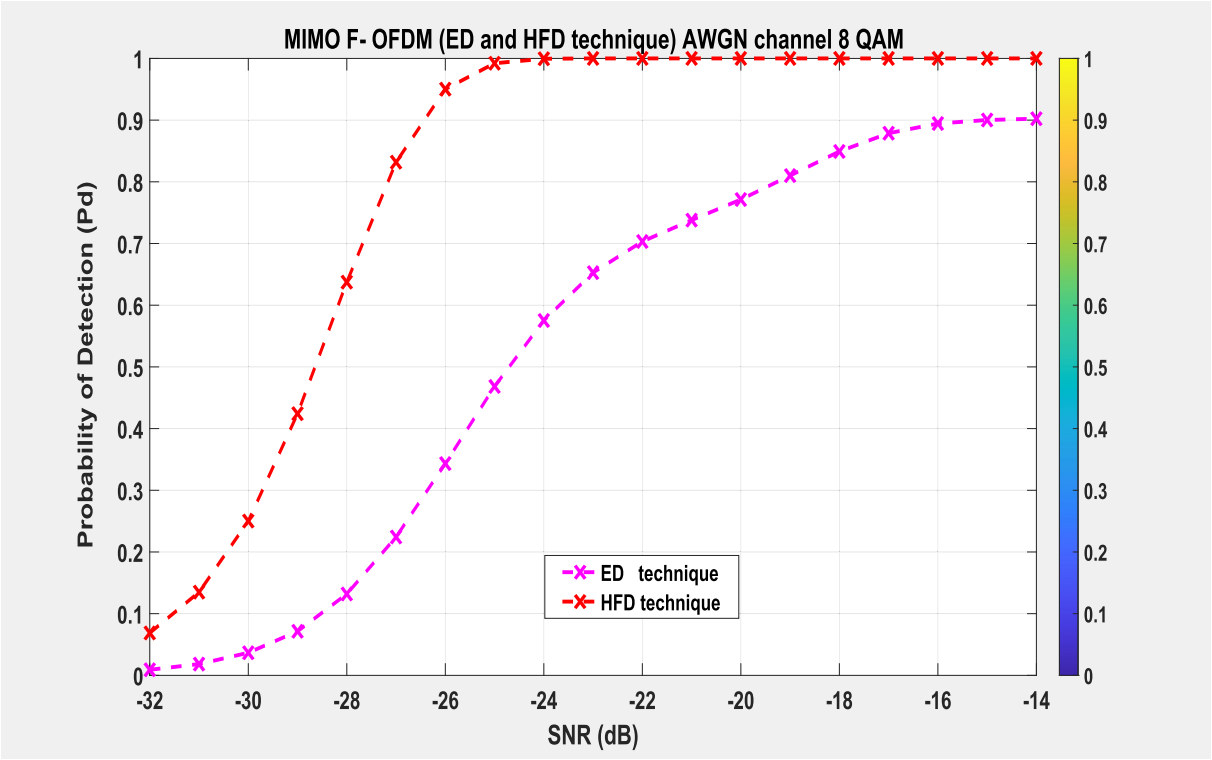

Fig. 18 Simulation results on AWGN channel based on the ED and HFD technique (8 QAM).

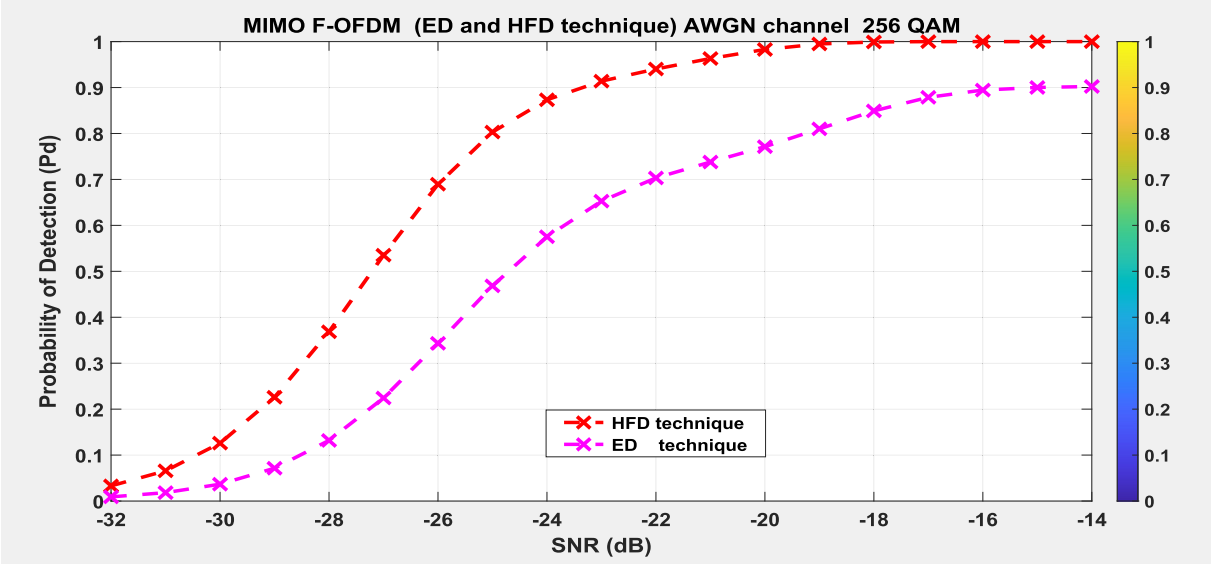

Fig. 19 Simulation results on AWGN channel based on the ED and HFD technique (256 QAM).

technique achieved 0.99 PD at −20 dB compared to −14 dB for ED. The outcomes indicate that higher modulation orders reduce detection probabilities.

10. Practical detection by USRP

The devised hybrid filter handles F-OFDM signals and follows CSS approach recommendations for reduced complexity. Moreover, the likelihood of a global false alert is minimal. Also, noise variance is significant for different 5G signals. The test is discussed comprehensively, and the outcomes are contrasted against simulation outcomes from MATLAB. The experiment evaluates how sample size impacts detection likelihood; noise modulation amplitude for GRC is between 4 and 50, creating an SNR range of −30 dB to 5 dB. The false alarm likelihood limit is set at 0.05 according to the IEEE 802.22 WRAN rules. The detection probability concerning a PU for one test is computed using 1000 iterations created from one

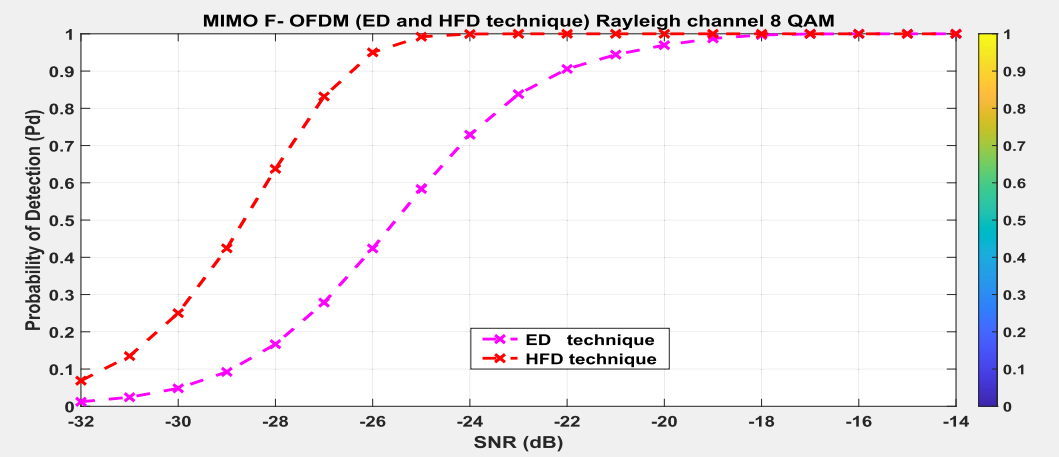

Fig. 20 Simulation results on Rayleigh channel based on the ED and HFD technique (8 QAM).

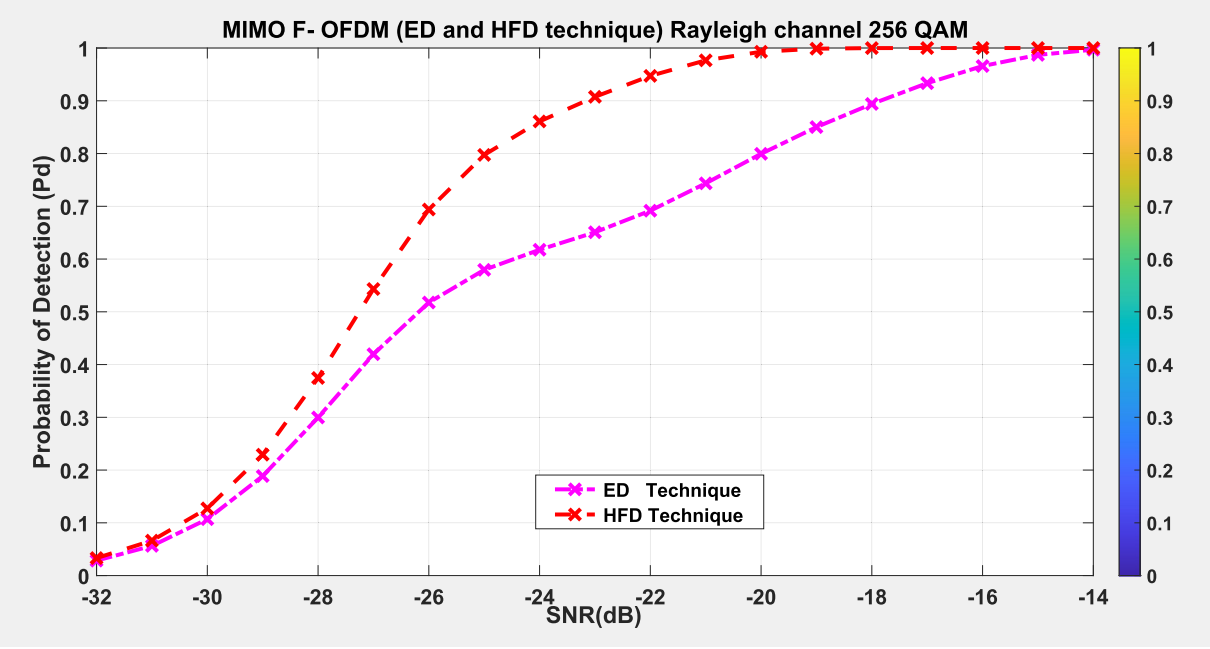

Fig. 21 Simulation results on Rayleigh channel based on the ED and HFD technique (256 QAM).

flow graph run. Estimation is improved using 10 experiment iterations and averaging the detection probability. A similar approach is followed for the required SNR values. Fig. 22 indicates an SNR plot and detection probability for different sample sizes (256, 512, 1024, and 2048). The graphed outcomes indicate the SNR and detection probability correlate direct, indicating a trend aligning with the simulation outcomes. Hence, a larger sample enhances detection probability.

As per Fig. 22, it is seen that detection probability increases with rise in signal-to-noise ratio. This suggests that with a rise in signal strength (with increase in signal-to-noise ratio), there is also an increase in the probability of identifying a PU. Increase in sample size also results in increase in detection probability.

Table 4, 5 and 6 demonstrates validation by comparing the probability of detection with different sample sizes between the practical and simulated experiment at (-24, −20, −16) dB. Based on table 4, the simulation achieved the required probability pertaining to detection (Pd $\geq$ 0.8) with N = 512, while the practical sensor would need a sample size of a minimum N = 2048 to attain the desired probability of detection. For the first time, the paper puts forward an HFD-based sensing method applied on USRP software. First, a new HFD-based sensing method is introduced by accounting for the physical property of sensing function, which provides a key enhancement with regards to detection performance. Second, derivation of analytical expressions pertaining to detection probability as well as false alarm probability is done, wherein the derived mathematical expressions were seen to match better with those of the conducted simulations. Various simulations have been conducted by assuming AWGN fading channel for demonstrating the effectiveness pertaining to

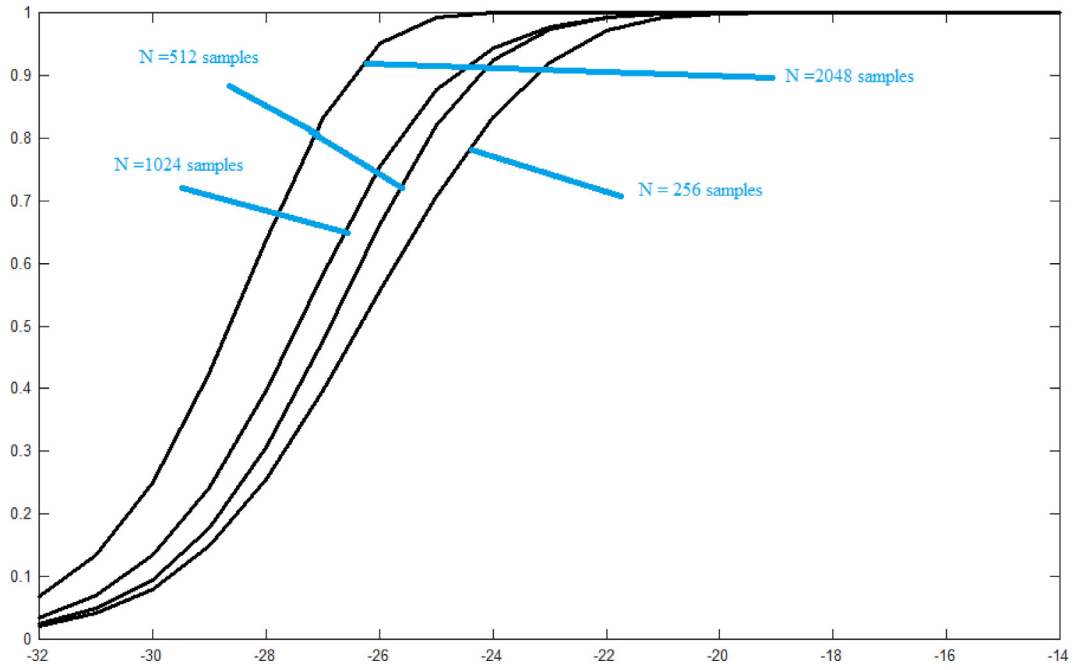

Fig. 22 Signal-to-Noise Ratio versus Probability of detection with varying Sample Size (P fa = 0.01) with hybrid filter.

Table 4 Performance comparison of simulation with implementation at −24 dB.

Sample Size (N)	256	512	1024	2048
Simulated (Pd)	0.78	0.91	0.95	0.996
practical (Pd)	0.80	0.91	0.93	0.995

Table 5 Performance comparison of simulation with implementation at −20 dB.

Sample Size (N)	256	512	1024	2048
Simulated (Pd)	0.95	0.989	0.99	0.99
Practical (Pd)	0.97	0.979	0.983	0.99

Table 6 Performance comparison of simulation with implementation at −16 dB.

Sample Size (N)	256	512	1024	2048
Simulated (Pd)	0.996	0.997	0.998	0.999
practical (Pd)	0.992	0.993	0.993	0.999

HFD-based sensing method. The HFD-based sensing methods were found to be more robust versus conventional ED-based sensing.

As demonstrated in Fig. 10, different scenarios have been designed based on the same setup for validating the implementation. Furthermore, a graphical interface has been realized considering all crucial parameters of HFD-based sensing (Pfa, Pd, FFT size, carrier centre frequency, and sample size).

Based on tables 4, 5, 6, the simulation was seen to achieve the required probabilities of detection (Pd = 0.91, Pd = 0.989, Pd = 0.997) when N = 512; (Pd = 0.78, Pd = 0.95, Pd = 0.996) when N = 256; (Pd = 0.95, Pd = 0.99, Pd = 0.998) when N = 1024; as well as (Pd = 0.996, Pd = 0.99, Pd = 0.999) when N = 2028 sequentially. However, a sample size of a minimum N = 2048 is needed for the practical sensor to attain the needed detection probability. This demonstrates that the practical system is not able to achieve the IEEE 802.22 WRAN standard's desired probability of detection when sample sizes are lesser than 2048. Smaller sample sizes result in lower probability of detection versus the simulation results. This is attributed to the thermal and channel noises in the USRP. Also, an analysis performed on the simulated and practical sensors demonstrated that the detector's performance was impacted by the sample size, thus suggesting a correlation between sample size and the performance of the hybrid filter detector. Based on the practical results, the lowest sample size of 2048 was determined, which could be employed aptly at the desired Pd and Pfa values. Furthermore, to assess the detection performance pertaining to HFD-based sensing methods in a real environment, an experimental setup is designed. Under the real channel, HFD-based sensing has been seen to outperform the ED-based sensing. Thus, the HFD-based sensing method offers certain interesting characteristics like a decreased detection sensing time and enhanced detection even under low SNR along with better resistance towards channel impairments, making this sensing technique an optimum candidate for CR applications.

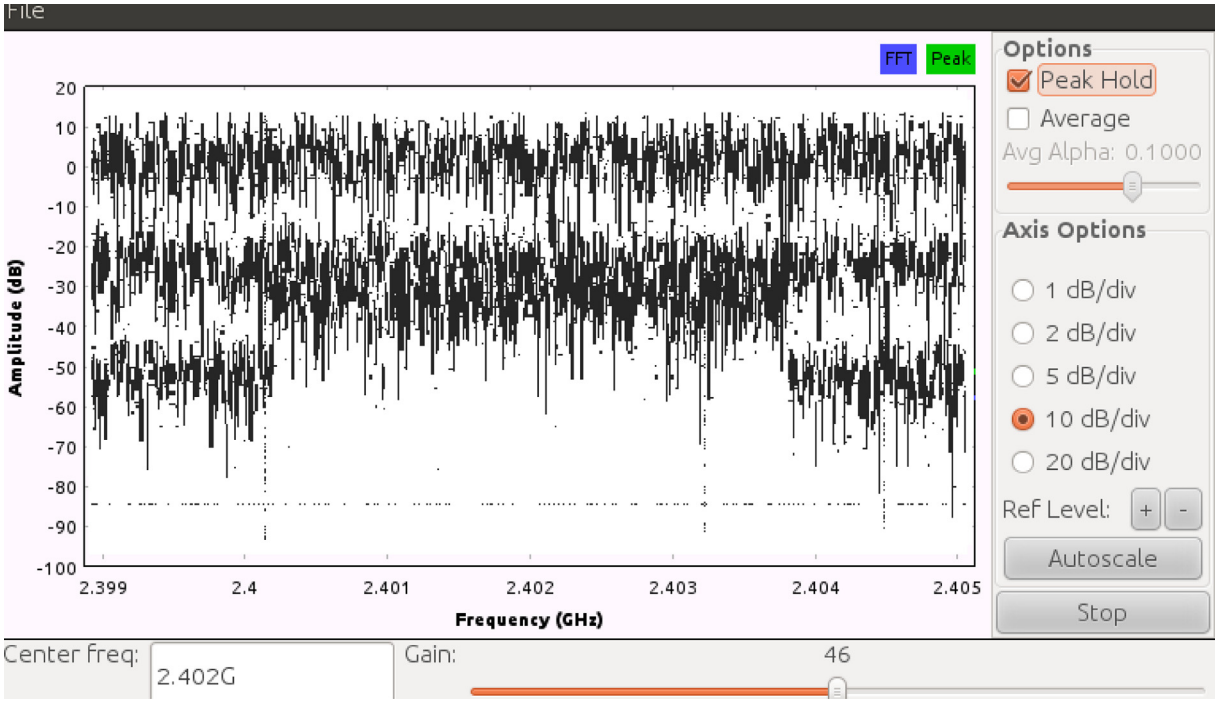

Fig. 23 The received signal power at center frequency = 2.40 GHz when the signal of the PU is present.

Also, a QAM signal that was centred on the 2.40 GHz carrier frequency from the experiment was evaluated. As demonstrated in Fig. 23, when the PU transmitter utilises the channel, the SU signal and power transmission occur on the receiver side.

Calculation of the threshold is done based on Eq. (13), which is employed for the ED algorithm. In GNU Radio, received signals can be observed based on the HFD block. Furthermore, at the SU, storing of the processed signal is done in a data file, which is applied to the detect upload block, and then, this data file is employed for analysis in MATLAB.

Fig. 24 shows the MIMO F-OFDM transmitted spectrum lacking any channel and preamble. Here, a low OOB power can be clearly seen, which is in the order of − 42 dB. This led not only to decrease in unwanted egress noise but also offer MIMO F-OFDM a chance to function with regards to scrambled spectrum applications [21]. Fig. 25 shows the actual spectrum that is received in the USRP, wherein amplitude distortion caused by multipath nature of wireless channels can be observed.

The latter experiments demonstrated the strength pertaining to the probability of detection sensing with regards to

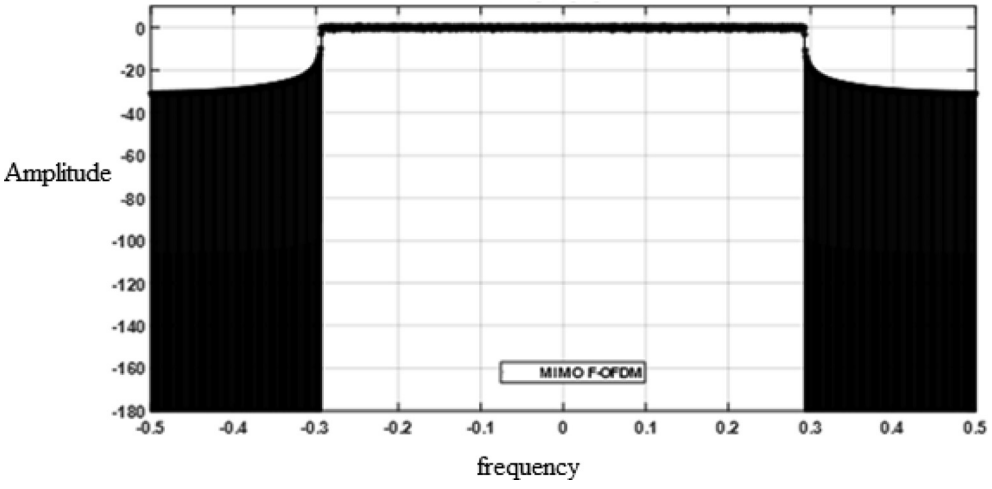

Fig. 24 MIMO F-OFDM spectrum with no degradation.

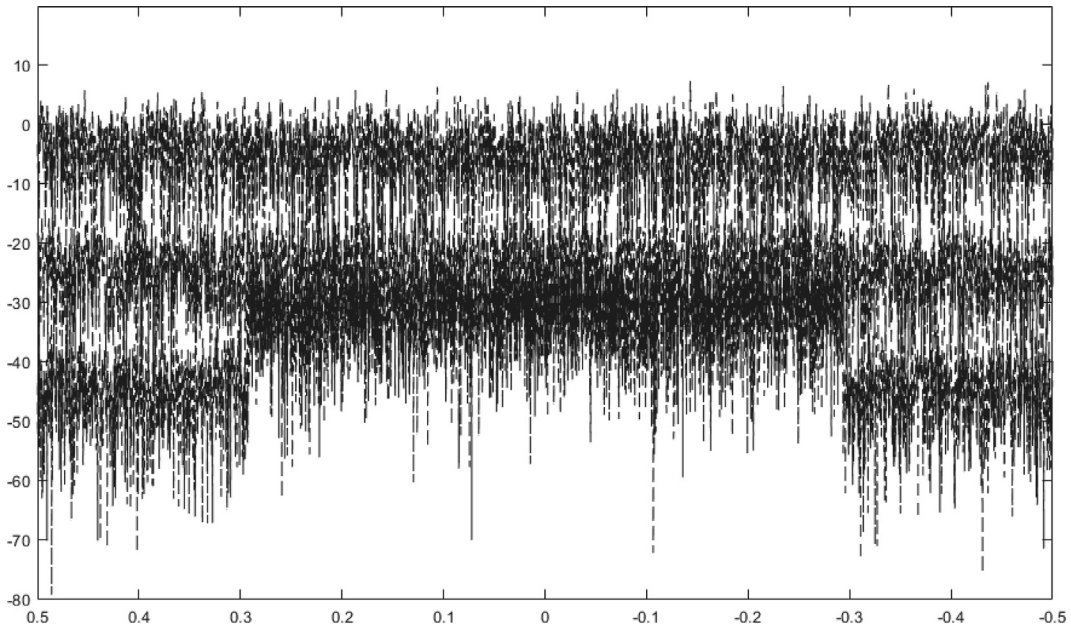

Fig. 25 MIMO F-OFDM spectrum with degradation.

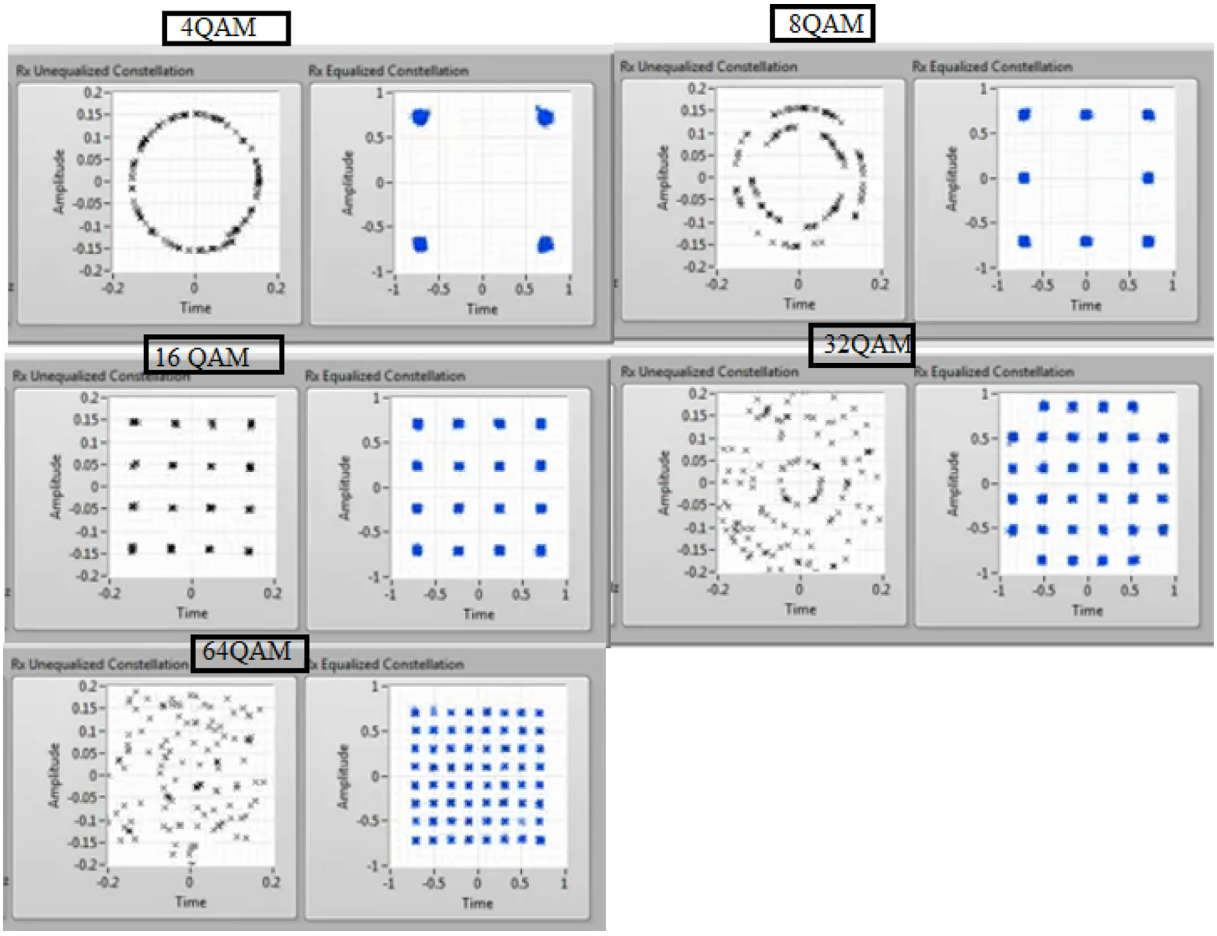

Fig. 26 MIMO- F-OFDM Sensing with SNR = -24 dB for [4 QAM, 8 QAM, 16 QAM, and 64 QAM].

CR applications. Besides, certain previous theoretical results have validated the effectiveness pertaining to HFD-based sensing under exposed to real environment.

In Fig. 26, the 5G F-OFDM signal was modulated at different M−ary QAM rates. The sensing characteristics were determined for 50 SUs at SNR value −24 dB. The specified 5G

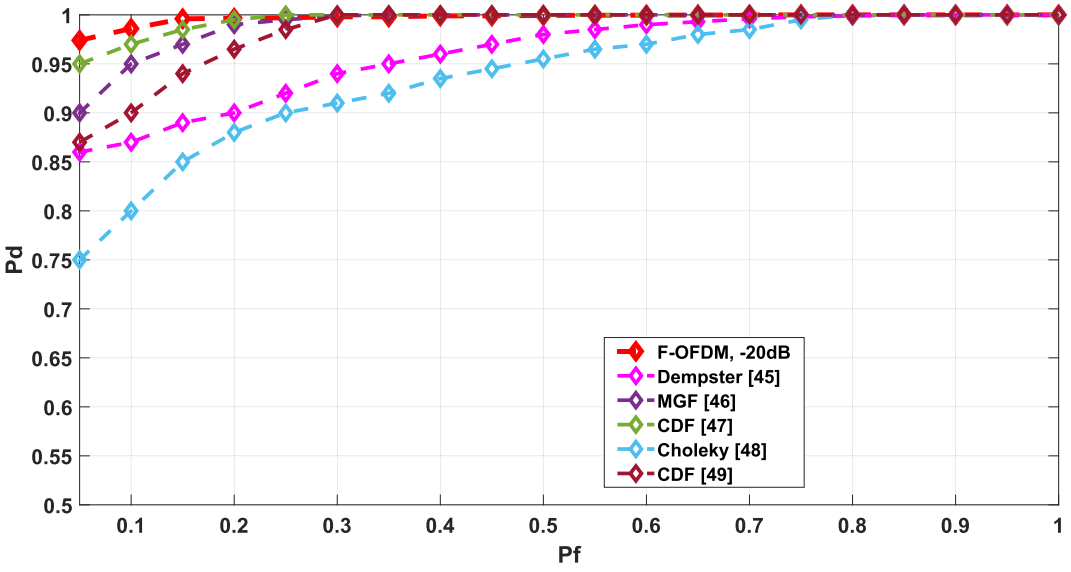

Fig. 27 false alarm probability 0.05, CSS, MIMO F-OFDM.

signal and the proposed framework were implemented using USRP. The figures depicted below indicate characteristics for 4QAM, 8QAM, 16QAM, 32QAM and 64QAM at −24 dB SNRs.

11. A comparison with related works

The simulation algorithm was validated using 1000 independent trials of MC simulation, and the results displayed that the F-OFDM waveform demonstrated the strongest detection performance, due to its short signal length and cancellation of null coefficients. Additionally, it was established that the SS system outperformed other techniques in different 5G waveform Additionally, it was revealed that the F-OFDM waveform needed less time for its detection process, as it had a shorter signal length. However, F-OFDM displayed better detection performance. In order to compare the systems, a low false alarm probability of 0.05 was adopted to maintain a low error rate probability (as indicated in Fig. 27). The parameters for F-OFDM 5G based waveform were selected based on their references, and typically rated. From Equations (9), (10), and (25), it can be seen that the length of signal V (number of samples) has a significant impact on the sensing parameters. Increasing the sample size will improve detection performance. The method provided in [46] achieved 0.96 detection probability, yet requiring coherency, pre-defined data such as frequency, and a highly sophisticated detection system. Moreover, it was unable to detect 5G signals when the SNR was below −6 dB. In [29], the same technique was utilized with different types of modulations, and the detection probability was 0.885. Although a few of their modulations could sense when SNR was −20 dB, they needed a complex detection system. The researchers utilized a distinct complex detection system in [44] that had a 0.868 detection probability, yet with the need for coherency and predetermined data values for waveform shapes and frequency. It showed good performance at SNRs > 10 dB, but it failed when SNR was under −10 dB. On the other hand, the covariance matrix suggested in [47] did not require any pre-defined data and achieved a 0.78 detection probability. However, this system employed the Cholesky-decomposition algorithm for signal detection and a RBF-

Table 7 The Parameters of 5G Waveform Kinds.

Parameters	ROC (P_f, P_d)	P_e	SNR Wall / *dB*	Complexity
Cyclostationarity Feature Detection [46]	0.05, 0.96	0.09	−6	High
Covariance Matrix Cholesky Decomposition	0.05, 0.78	0.27	−15	Moderate
Cyclostationarity Feature Detection [29]	0.05, 0.885	0.165	−20	High
Dempster-Shafer Fusion [44]	0.05, 0.868	0.182	−10	High
Moment Generating Function [45]	0.05, 0.93	0.12	10	Moderate
Windowed Cosine Filter-Bartlett-Hamming	0.05, 0.971 (for F-OFDM) 0.05, 0.955 (for UFMC) 0.05, 0.977 (for FBMC)	0.079 (for F-OFDM) 0.095 (for UFMC) 0.073 (for FBMC)	–32	Low
Comparison	The proposed method has a better sensing performance	The proposed method has a lower system error	The proposed method can work for a lower SNR	The proposed method has a simpler design

based vector machine algorithm for making decisions, resulting in a moderate complexity level. Yet, it was not sufficient for low false alarm probability and SNR below −15 dB. In [45], the researchers utilized a moment generating function algorithm with multi-antenna in order to gain 0.93 detection probability. With the complexity increase, the system was unable to function for SNR less than 10 dB. The SS system proposed in this paper was able to surmount the SNR wall with its low complexity and low error rate. Furthermore, it showed significant results for different 5G waveform and managed to differentiate between traffic and AWGN noise despite.

Table 7 summarizes the best rates of the proposed SS system and other related works for some parameters. It was observed that the SS system achieved superior accuracies in detection and false-alarm compared to other studies.Consequently, the proposed SS system boasted a higher detection probability, reduced false alarm rate, and improved error probability. The proposed SS system demonstrated the lowest complexity due to its reliance on basic operations such as addition and subtraction, compared to the techniques in [46,29], and [44] that had higher computational complexity based on integration and other similar operations. It was also observed that [45] and [47] had a moderate complexity since several operations were necessary for the signal detection process. Therefore, the system could effectively detect signals in low SNR (-20 dB) conditions compared to the others.

12. Conclusion

In this paper, the performance of the SS technique for centralized cooperative (secondary users) method. the system was performed for the 5G-MIMO communications system with a number of antennas for both transmitter and receiver. one kind of 5G systems has been analyzed; F-OFDMMIMO, system. The mathematical expressions are proposed for various numbers of secondary users, transmitter and receiver antennas, length of signal, and waveform shapes. Besides, developing the impact of test statistic and signal length rather than the expressions of detection for false alarm probabilities for the centralized cooperative users are analyzed too. The obtained results of simulation for different number of samples, different values of SNRs, and the modulation types. The proposed system overcome the issues of low SNRs, and F-OFDM-MIMO system. The best results are obtained as follows; probability of detection for F-OFDM MIMO (for 50 users). On the other hand, the increased number of antennas enhanced the detection performance in comparison with other detection systems that are did not use the MIMO technique. Also This paper offers a comprehensive analysis to assess the performance pertaining to MIMO (2 × 2) F-OFDM systems with regards to detection and transmission of message bits. The simulation results showed that the hybrid filter detector could identify signals as low as −24 dB at the intended probability of detection of 0.98, and likelihood of false alarm at 0.01, with a sample size of 2048. By keeping the parameters same, the lowest detectable experimental practical SNR was −20 dB. This demonstrated lower efficiency of the practical sensor by almost −16 dB, and the finest detection performance is attained when M−ary = 4 and number of SUs = 50 user, while the worst detection performance is attained when M−ary = 256 and number of SUs = 10 user. Going forward, the developed MIMO-F-OFDM demonstrator would be assimilated into the NI 6G Application Framework. This solution would help in further probing on the elasticity of F-OFDM with regards to resource management and scheduling algorithms employed by the MAC layer.

Declaration of Competing Interest

The authors declare that they have no known competing financial interests or personal relationships that could have appeared to influence the work reported in this paper.

Acknowledgements

We thank Dr. Hussein Al-Sheakh of University of Michigan / United States of America for help us in laboratory.

Appendix:. See Table A1.

Table A1 Main parameters.

Notation / Abbreviations	*Description*
H_0	Null hypothesis
H_1	Alternative hypothesis
$x[v]$	Transmitted 5G (PU) signal (it is either F-OFDM, UFMC, or FBMC)
P_f	Probability of false-alarm
PU	Primary user
SU	Secondary user
P_{md}	Probability of miss-detection
P_e	Probability of system error
SS	Spectrum sensing
SNR	Signal-to-noise ratio
Ho	Null hypothesis
$H1$	Alternate hypothesis
MC	Monte-Carlo
P_d	Probability of detection
$r[v]$	Received 5G (PU) signal
$w[v]$	Noise
V	Original received signal length
σ_w^2	Noise variance
σ_s^2	Signal variance
Λ	Decision statistic
$\Phi_{H0}(\eta)$	Cumulative Distribution Function of λ under H_0
$\Phi_{H1}(\eta)$	Cumulative Distribution Function of λ under H_1
H	Predefined threshold
$R'_{F\text{-}OFDM}[k]$	Transformed received F-OFDM signal based 5G after removing null coefficients
$R_{F\text{-}OFDM}[k]$	Transformed received F-OFDM signal based 5G
s_n^b	Transmitted data
$g[l]$	Frequency corresponding to the finite impulse response prototype filter
$R[0]$	First element of the transformed signal
$R[k]$	Other elements of the transformed signal
K	Transformed received signal length (corresponding to the original received signal length)

Table A1 (*continued*)

Notation / Abbreviations	*Description*
K'	New transformed received signal length after removing null coefficients
Θ	Ratio of original signal length to the new signal length
A	SNR
USRP	Universal Software Radio Peripheral
AWGN	Additive White Gaussian Noise
FPGA	Field Programmable Gate Array
ROC	Receiver Operating Characteristics
FCC	Federal Communication Commission
CSS	Cooperative spectrum sensing
SS	Spectrum sensing

References

[1] Yurui Cao; Sai Xu; Jiajia Liu; Nei Kato, "Toward Smart and Secure V2X Communication in 5G and Beyond: A UAV-Enabled Aerial Intelligent Reflecting Surface Solution," IEEE Vehicular Technology Magazine (2022) (Volume: 17, Issue: 1, March 2022). 10.1109/MVT.2021.3136832.

[2] J.A.H. Sánchez, K. Casilimas, O.M.C. Rendon, Deep reinforcement learning for resource management on network slicing: a survey, Sensors 22 (2022) 3031, https://doi.org/10.3390/s22083031.

[3] Mohammad Alibakhshikenari; Bal S. Virdee; Chan Hwang See; Pancham Shukla; Sadegh Mansouri Moghaddam; Ashraf Uz Zaman; Samia Shafqaat; Mobayode O. Akinsolu; Bo Liu; Jian Yang; Raed Abd-Alhameed; Francisco Falcone; Ernesto Limiti, "Dual-Polarized Highly Folded Bowtie Antenna with Slotted Self-Grounded Structure for Sub-6 GHz 5G Applications", IEEE Transactions on Antennas and Propagation (Volume: 70, Issue: 4, April 2022). DOI: 10.1109/TAP.2021.3118784.

[4] Arun Kumar, Sumit Chakravarty, S. Suganya, Himanshu Sharma, Rajneesh Pareek, Mehedi Masud, Sultan Aljahdali , "Intelligent conventional and proposed hybrid 5G detection techniques",Alexandria Engineering Journal, volume 61, Issue 12, December 2022, Pages 10485-10494. https://doi.org/10.1016/j.aej.2022.04.002.

[5] Zeba Idrees; Muhammad Usman; Hasan Erteza Gelani; Lirong Zheng, "Fast and Robust Spectrum Sensing for Cognitive Radio Enabled IoT", IEEE Access (volume: 9), page(s): 165996 - 166007. DOI: 10.1109/ACCESS.2021.3133336.

[6] L.B. Le, V. Lau, E. Jorswieck, et al, Enabling 5G mobile wireless technologies, J Wireless Com Network (2015) 218, https://doi.org/10.1186/s13638-015-0452-9.

[7] D. Borges, P. Montezuma, R. Dinis, M. Beko, Massive MIMO Techniques for 5G and Beyond—Opportunities and Challenges, Electronics 10 (2021) 1667, https://doi.org/10.3390/electronics10141667.

[8] A. Kumar, M. Gupta, A review on activities of fifth generation mobile communication system Author links open overlay panel, Alexandria Engineering Journal 57 (2) (2018) 1125–1135, https://doi.org/10.1016/j.aej.2017.01.043.

[9] A. Kumar, a, R. Dhanagopal b, Mahmoud A., Albreem c, Dac-Nhuong Le, "A comprehensive study on the role of advanced technologies in 5G based smart hospital", Alexandria Engineering Journal 60(6) (2021) 5527–5536, https://doi.org/10.1016/j.aej.2021.04.016.

[10] S. Lin, B. Zheng, F. Chen, R. Zhang, " Intelligent Reflecting Surface-Aided Spectrum Sensing for Cognitive Radio, IEEE Wireless Communications Letters (2022). https://doi.org/10.48550/arXiv.2202.02550.

[11] Zachary Bosire Omariba, "Analysis of spectrum allocation of secondary users based on linear cooperative spectrum sensing techniques in cognitive radio networks, Trends in Computer Science and Information Technology, 14 April, (2021), https://doi.org/10.17352/tcsit.000035.

[12] Antonio Brito, Pedro Sebastião, Fernando José Velez, "Hybrid Matched Filter Detection Spectrum Sensing, December (2021), IEEE Access PP(99):1-1,DOI:10.1109/ACCESS.2021.3134796.

[13] F. Conceição, M. Gomes, V. Silva, R. Dinis, A. Silva, D. Castanheira, A Survey of Candidate Waveforms for beyond 5G Systems, Electronics 10 (1) (2021) 21, https://doi.org/10.3390/electronics10010021.

[14] M. Alibakhshikenari, B.S. Virdee, P. Shukla, C.H. See, R.A. Abd-Alhameed, Francisco Falcone, Karim Quazzane, Ernesto Limiti, " Isolation enhancement of densely packed array antennas with periodic MTM-photonic bandgap for SAR and MIMO systems", IET Microwaves, Antennas & Propagation Vol. 14 Iss. 3 (2020) 183–188, https://doi.org/10.1049/iet-map.2019.0362.

[15] M. Banafaa, I. Shayea, J. Din, Marwan Hadri Azmi, Abdulaziz Alashbi, Yousef Ibrahim Daradkeh, Abdulraqeb Alhammadi, "6G Mobile Communication Technology: Requirements, Targets, Applications, Challenges, Advantages, and Opportunities", Alexandria Engineering Journal 64 (1) (February 2023) 245–274, https://doi.org/10.1016/j.aej.2022.08.017.

[16] Keesara Upender Reddy, "Spectrum Sensing of FBMC Signals in 5G and, Cognitive Radios (2018). https://faculty.iiit.ac.in.

[17] A. Kumar, S. Saha, A decision confidence based multiuser MIMO cooperative spectrum sensing in CRNs, Physical Communication 39 (2020), https://doi.org/10.1016/j.phycom.2019.100995 100995.

[18] W. Lee, M. Kim, D.-H. Cho, Deep cooperative sensing: Cooperative spectrum sensing based on convolutional neural networks, IEEE Transactions on Vehicular Technology 68 (3) (2019) 3005–3009, https://doi.org/10.1109/TVT.2019.2891291.

[19] S. Yu et al, Adaptive double-threshold cooperative spectrum sensing algorithm based on history energy detection, Wireless Communications and Mobile Computing (2020), https://doi.org/10.1155/2020/4794136.

[20] T. Balachander, M. Krishnan, Efficient Utilization of Cooperative Spectrum Sensing (CSS) in Cognitive Radio Network (CRN) Using Non-Orthogonal Multiple Access (NOMA), Wireless Personal Communications (2021) 1–22, https://doi.org/10.1007/s11277-021-08776-7.

[21] M.K. Giri, S. Majumder, Eigenvalue-based cooperative spectrum sensing using kernel fuzzy c-means clustering, Digital Signal Processing 111 (2021), https://doi.org/10.1016/j.dsp.2021.102996 102996.

[22] M.S. Miah a,b,*, M. Schukat a, E. Barrett a, "Sensing and throughput analysis of a MU-MIMO based cognitive radio scheme for the Internet of Things, (2020), https://doi.org/10.1016/j.comcom.2020.03.003.

[23] Dey, Ciuonzo, P. Salvo Rossi, Wideband Collaborative Spectrum Sensing using Massive MIMO Decision Fusion, (2020), IEEE TRANSACTIONS ON WIRELESS COMMUNICATIONS, APR. 2020. 10.1109/TWC.2020.2991113.

[24] T. Balachander · M. B. Mukesh Krishnan, "Efficient Utilization of Cooperative Spectrum Sensing (CSS) in Cognitive Radio Network (CRN) Using Non orthogonal Multiple Access (NOMA) (2021), Wireless Personal Communications, https://doi.org/10.1007/s11277-021-08776-7.

[25] G uman Kanwar SHekhawat, R.P. Yadav,, "Sparse Code Multiple Access based Cooperative Spectrum Sensing in 5G Cognitive Radio Networks, in: 5th International Conference on

Computing, Communication and Security (ICCCS), https://doi.org/10.1109/ICCCS49678.2020.9276888.
[26] R. Sowmiya, G. Sangeetha, Energy detection using NI USRP 2920, International Journal of Science and Research 5 (5) (2016) 597–603, https://doi.org/10.21275/v5i5.nov163414.
[27] A. Nafkha, M. Naoues, K. Cichon, A. Kliks, "Experimental Spectrum Sensing Measurements using USRP Software Radio Platform and GNU-Radio,, June 02–04, Oulu, Finland (2014), https://doi.org/10.4108/icst.crowncom.2014.255415.
[28] C.-L. Tai, S.u. Borching, C. Jia, "Frequency-Domain Decoupling for MIMO-GFDM Spatial Multiplexing, IEEE (2018), https://doi.org/10.48550/arXiv.1803.06448.
[29] W.M. Jang, Simultaneous Power Harvesting and Cyclostationary Spectrum Sensing in Cognitive Radios, IEEE Access 8 (2020) 56333–56345, https://doi.org/10.1109/ACCESS.2020.2981878.
[30] H. Xing, H. Qin, S. Luo, P. Dai, L. Xu, X. Cheng, "Spectrum sensing in cognitive radio: A deep learning based model, Trans Emerging Tel Tech. 33 (1) (2022), https://doi.org/10.1002/ett.4388 c4388.
[31] Tala Talaei Khoei, Shereen Ismail, Naima Kaabouch, "Dynamic Selection Techniques for Detecting GPS Spoofing Attacks on UAVs, Sensors 22 (2) (2022) 662, https://doi.org/10.3390/s22020662.
[32] Shaoe Lin, Beixiong Zheng, Fangjiong Chen, and Rui Zhang, "Intelligent Reflecting Surface-Aided Spectrum Sensing for Cognitive Radio, IEEE WIRELESS COMMUNICATIONS LETTERS (2022), http://arxiv.org/abs/2202.02550v1.
[33] Youness Arjoune* and Naima Kaabouch, "A Comprehensive Survey on Spectrum Sensing in Cognitive Radio Networks: Recent Advances, New Challenges, and Future Research Directions Sensors (Basel). (2019) Jan; 19(1): 126. doi: 10.3390/s19010126.
[34] Mohammad Hossein Same , Gabriel Gandubert, Gabriel Gleeton, Preslav Ivanov and René Landry, Jr., SimplifiedWelch "Algorithm for Spectrum Monitoring, 24 December (2020) , https://dx.doi.org/10.3390/app11010086.
[35] H. Li, H.u. Yanzhu, S. Wang, "Signal Detection Based on Power-Spectrum Sub-Band Energy Ratio, Electronics 10 (2021) 64, https://doi.org/10.3390/electronics10010064.
[36] Josip Lorincz, Ivana Ramljak and Dinko Begušĭc , "Analysis of the Impact of Detection Threshold Adjustments and Noise Uncertainty on Energy Detection Performance in MIMO-OFDM Cognitive Radio Systems, Sensors(2022), 22(2), 631; https://doi.org/10.3390/s22020631.
[37] Abbass Nasser , Hussein Al Haj Hassan , Jad Abou Chaaya , Ali Mansour, Koffi-Clément Yao, "Spectrum Sensing for Cognitive Radio: Recent Advances and Future Challenge, Sensors (2021), 21, 2408. https://doi.org/10.3390/ .
[38] J. Yli-Kaakinen, A.E. Loulou, T. Levanen, K. Pajukoski, A. Palin, M. Renfors, M. Valkama, Frequency-Domain Signal Processing for Spectrally-Enhanced CP-OFDM Waveforms in 5G New Radio, IEEE Transactions on Wireless Communications (2021). https://arxiv.org/abs/2008.00672, https://doi.org/10.1109/TWC.2021.3077762.
[39] H. Chen, J. Hua, J. Wen, K. Zhou, J. Li, D. Wang, X. You, Uplink interference analysis of F-OFDM systems under non-ideal synchronization, IEEE Transactions on Vehicular Technology 69 (12) (2020) 15500–15517, https://doi.org/10.1109/TVT.2020.3041938.
[40] J. Khan, S. Ullah, U. Ali, Farooq Ahmad Tahir, Ildiko Peter, and Ladislau Matekovits, "Design of a Millimeter-Wave MIMO Antenna Array for 5G Communication Terminals, Sensors 22 (2022) 2768, https://doi.org/10.3390/s22072768.
[41] A. Vega, E. Alejandro, A.L.S. Orozco, L.J.G. Villalba, J. Hernandez-Castro, Digital images authentication technique based on dwt, dct and local binary patterns, Sensors 18 (10) (2018) 3372, https://doi.org/10.3390/s18103372.
[42] Z. Hua, Y. Zhou, H. Huang, Cosine-transform-based chaotic system for image encryption, Information Sciences 480 (2019) 403–419, https://doi.org/10.1016/j.ins.2018.12.048.
[43] https://kb.ettus.com/About_USRP_Bandwidths_and_Sampling_Rates.
[44] X. Liu, M. Jia, Z. Na, W. Lu, F. Li, Multi-modal cooperative spectrum sensing based on dempster-shafer fusion in 5G-based cognitive radio, IEEE Access 6 (2017) 199–208.
[45] G. Chu, K. Niu, W. Wu, F. Yang, MGF-based analysis of spectrum sensing over K-μ fading channels for 5G cognitive networks, IEEE Access 6 (2018) 78650–78658.
[46] N.A. El-Alfi, H.M. Abdel-Atty, M.A. Mohamed, Sub- Nyquist cyclostationary detection of GFDM for wideband spectrum sensing, IEEE Access 7 (2019) 86403–86411, https://doi.org/10.1109/ACCESS.2019.2925047.
[47] J. Bao, J. Nie, C. Liu, B. Jiang, F. Zhu, J. He, Improved blind spectrum sensing by covariance matrix Cholesky decomposition and RBF-SVM decision classification at low SNRs, IEEE Access 7 (97117) (2019) 97129, https://doi.org/10.1109/ACCESS.2019.2929316.